Determination of permeability from spectral induced polarization in granular media

A. Revil, Nicolas Florsch

Geophysical Journal International

Determination of permeability from spectral induced polarization in granular media

A. Revil[1,2] and N. Florsch[3,4]

[1]*Department of Geophysics, Colorado School of Mines, Golden,* CO 80401, *USA.* E-mail: arevil@mines.edu
[2]*CNRS-UMR* 5559-LGIT, *Université de Savoie, Equipe volcan,* 73376 *Le-Bourget-du-Lac, France*
[3]*UPMC/IRD UMMISCO UMI* n°209, 32 Av. *Henry Varagnat,* 93143 *Bondy cedex, France*
[4]*Department of Mathematics and Applied Mathematics, University of Cape Town, South Africa*

SUMMARY

The surface conductivity of porous rocks has two contributions: the first is associated with the diffuse layer coating the grains and is frequency-independent as long as the diffuse layer is above a percolation threshold. The second contribution is associated with the Stern layer of weakly sorbed counterions on the mineral surface and is frequency-dependent if the Stern layer is discontinuous at the scale of the representative elementary volume. In the frequency range 1 mHz–100 Hz, this second contribution is also associated with the main polarization mechanism observed by the spectral induced polarization method in granular media (neglecting the contribution of other polarization processes like those associated with redox processes and membrane polarization). At the macroscale, we connect the Stern layer contribution to the complex conductivity and to the expectation of the probability distribution of the inverse of the grain size. This is done by performing a convolution between the probability distribution of the inverse of the grain size and the surface conductivity response obtained when all the grains have the same size. Surface conductivity at the macroscopic scale is also connected to an effective pore size used to characterize permeability. From these relationships, a new equation is derived connecting this effective pore size, the electrical formation factor, and the expected value of the probability distribution for the inverse of the grain size, which is in turn related to the distribution of the relaxation times. These new relationships are consistent with various formula derived in the literature in the limit where the grain size distribution is given by the delta function or a log normal distribution and agree fairly well with various experimental data showing also some limitations of the induced polarization method to infer permeability. One of these limitations is the difficulty to detect the relaxation, in the phase, associated with the smaller grains, as this polarization may be hidden by the Maxwell–Wagner polarization at relatively high frequencies (>100 Hz). Also, cemented aggregates of grains can behave as coarser grains.

Key words: Probability distributions; Electrical properties; Hydrogeophysics; Permeability and porosity.

1 INTRODUCTION

In the last decade, there has been a renewal of interest in the spectral induced polarization method (also called complex resistivity, complex conductivity, or low frequency dielectric spectroscopy) in near surface geophysics to image and characterize non-intrusively ground chemical and transport properties (Börner *et al.* 1996; de Lima & Niwas 2000; Slater & Lesmes 2002a,b; Binley *et al.* 2005; Hördt *et al.* 2007; Nordsiek & Weller 2008) and drying (Cosenza *et al.* 2007; Ghorbani *et al.* 2009). However, induced polarization, like attenuation in seismic, is notoriously difficult to interpret quantitatively because of the superposition of various types of po-

larization mechanisms, which may overlap in the frequency domain (Olhoeft 1985; Cosenza *et al.* 2008; Leroy *et al.* 2008; Leroy & Revil 2009; Jougnot *et al.* 2010). In metal-free and bacteria-free porous media, three main mechanisms seem to control induced polarization. (1) The polarization of the Stern layer coating the mineral surface is playing an important role as first shown by Schwarz (1962). (2) The Maxwell–Wagner polarization represents the blocking of the ions at dielectric boundary layers in heterogeneous materials like porous media (Maxwell 1892; Wagner 1914). This second contribution is related to the discontinuity of the displacement current at the interfaces between different phases. (3) The membrane polarization which corresponds to an extension of the membrane potential

GJI Marine geosciences and applied geophysics

of self-potential theory (see Revil *et al.* 1999) to the frequency domain (Marshall & Madden 1959).

The polarization of the Stern layer arises in a wide frequency range from 1 mHz to 100 Hz and is controlled by the grain size distribution (Leroy *et al.* 2008) while the Maxwell–Wagner polarization occurs at higher frequencies (usually >10 Hz) (Chen & Or 2006) and is controlled by the formation factor, the surface conductivity, and the dielectric properties of the different phases. The membrane polarization will not be considered in this paper. It certainly deserves a dedicated research work and to our knowledge only the work of Vinegar & Waxman (1984) has considered membrane polarization and double layer polarization together using a semi-empirical approach.

In this paper, we will consider only the polarization of the Stern layer assuming that the two other contributions can be safely removed from the total (measured response) or that the electrochemical polarization of the Stern layer is the main polarization mechanism in the frequency band considered, typically 1 mHz–10 Hz (see Leroy *et al.* 2008 for few examples showing potential distinct signatures for the three contributions discussed above). We will demonstrate that when this is the case, the complex conductivity or resistivity response can be tied to hydraulic parameters.

The potential relationship between permeability and complex conductivity has recently been one of the main drivers of scientific works on induced polarization. A number of researchers have shown that spectral induced polarization is sensitive to hydraulic parameters and may offer a non-intrusive method to image permeability in the field, at least in cases where no other polarization mechanisms could mask the polarization contribution responsible for this relationship. Works have been done showing that spectral induced polarization can be used, for instance, to determine the mean grain size, the mean pore size, the specific surface area, and the permeability of natural and artificial porous media (Börner & Schön 1991; Sturrock 1999; Lesmes & Morgan 2001; Titov *et al.* 2002; Scott & Baker 2003, 2005; Binley *et al.* 2005; Kemna *et al.* 2005; Tong *et al.* 2006a,b; Leroy *et al.* 2008). Unfortunately, none of these works offered a mechanistic understanding for these relationships. Recently, De Lima & Niwas (2000) proposed a model to explain the data reported by Vinegar & Waxman (1984) and the connection between complex conductivity parameters and permeability. However, their approach is based on a polarization mechanism of the diffuse layer that is difficult to accept because usually the diffuse layer is above a percolation level at the scale of the representative elementary volume and therefore would hardly polarize.

In this paper, we build first a new relationship between the main relaxation time derived from spectral induced polarization and permeability for porous media characterized by a delta function for the grain size distribution. Then, we generalize this approach to the case of an arbitrary grain size distribution and look at the other limiting case of a broad grain size distribution. We apply the resulting new relationships to various datasets to check their predictive power regarding their capacity to predict permeability for the two extreme cases of very narrow or very broad grain size distributions.

2 THEORETICAL BACKGROUND

2.1 The electrical double layer

Before describing surface conductivity and its frequency dependence, we need to review the concept of the electrical double layer,

which coats the surface of insulating grains with a special emphasis on silica and alumino-silicates. All minerals that are in contact with water develop a net surface charge on their surface because of the chemical reactivity of surface sites like silanol groups in the case of silica and silanol, aluminol, and isomorphic substitutions in the case of clays. This charge is counterbalanced by charges that are more or less weakly sorbed onto the mineral surface in a monolayer called the Stern layer. This layer is situated between the o-plane and the d-plane of Fig. 1. The o-plane corresponds to the true mineral surface while the d-plane corresponds to the inner surface of the electrical diffuse layer. The existence of this Stern layer is consistent with molecular dynamic simulations of the electrical double layer (see recently Tournassat *et al.* 2009). The surface charge plus the charge of the Stern layer are counterbalanced by charges located in the electrical diffuse layer where charge carriers are only subjected to the Coulombic force (Fig. 1). The result is that the activity of the counterions (the counterions are characterized by charges that are opposite to the fixed charge of the mineral surface) and the co-ions (same charge) in the diffuse layer obey a Boltzmann distribution in the Coulombic field created by the fixed charge on the grain surface. Revil & Leroy (2004) introduced a partition coefficient of the counter-charge between the Stern and the diffuse layers, f (dimensionless). This partition coefficient f can be computed as

$$f = \frac{\sum_{i=1}^{Q} q_i \Gamma_i^S}{\sum_{i=1}^{Q} q_i \Gamma_i^S + \sum_{i=1}^{Q} q_i \Gamma_i^d}, \tag{1}$$

where Q is the number of possible ionic species i that are present in the Stern layer and in the diffuse layer, q_i is the charge of species i (in C, positive or negative), Γ_i^S represents the surface site density of species i in the Stern layer (number of species i per unit surface area of the mineral water interface in m^{-2}), and Γ_i^d represents the equivalent surface site density of the diffuse layer (equivalent number of ion i of the diffuse layer per unit surface area of the mineral water interface, in m^{-2}).

We define also a total charge density of counterions per pore volume Q_V (in C m^{-3}). This charge density is the net charge density of the pore water from the o-plane to the centre portion of the pore space, therefore including the Stern layer. It comprises two contributions: the charge density due to the existence of the Stern layer and the charge density due to the diffuse layer. We denote $\bar{Q}_V$ (in C m^{-3}) as the charge density per unit of volume of solution in the medium due to the diffuse layer only. These two charge densities are phase average of the local charge density. They are related to each other by the partition coefficient f defined through the following relationship:

$$\bar{Q}_V = (1 - f) Q_V, \tag{2}$$

and Q_V can be determined from the Cation Exchange Capacity (CEC, expressed in C kg^{-3}) of the rock

$$Q_V = \rho_S \left(\frac{1 - \phi}{\phi} \right) \text{CEC}, \tag{3}$$

where ρ_S is the mass density of the solid phase (in kg m^{-3}) and ϕ is the connected porosity. The CEC accounts for the charges sorbed onto the mineral surface (diffuse and Stern layers). It can be obtained from a simple chemical titration of the mineral surface (see Yukselen & Kaya 2008 and references therein). Because clays have large specific surface areas, they usually carry most of the CEC.
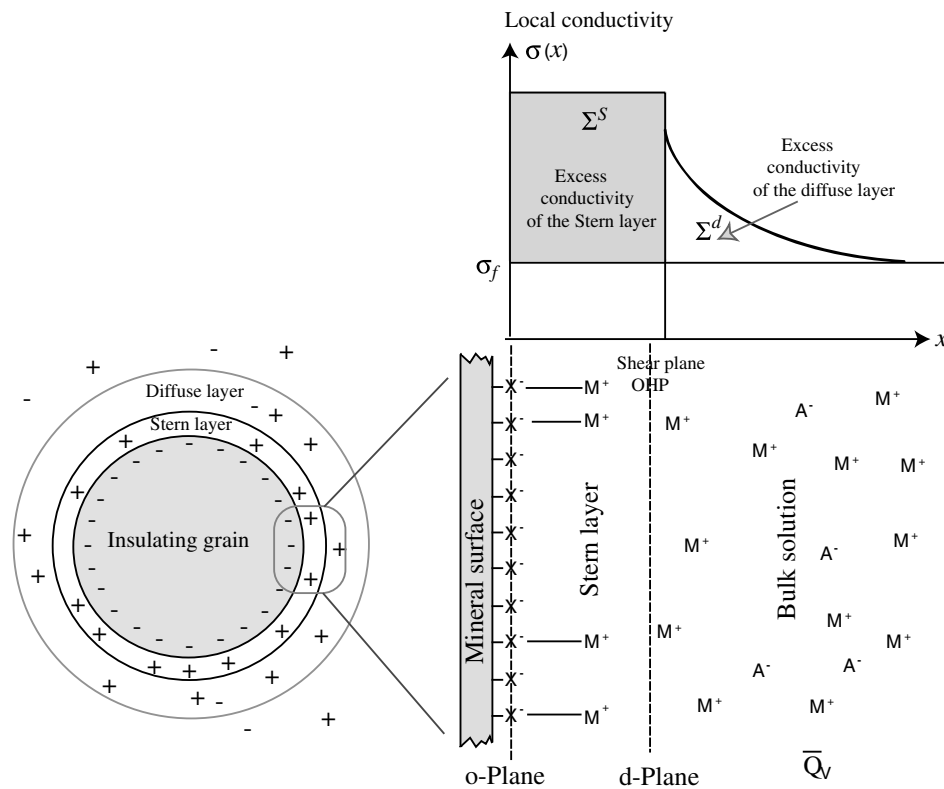
Figure 1. Sketch of the distribution of the ionic species in the pore space of a charged porous medium at equilibrium. The pore water is characterized by a volumetric charge density $\bar{Q}_V$ corresponding to the charge of the diffuse layer per unit pore volume (in C m^{-3}). The Stern layer is responsible for the excess surface conductivity Σ^S (in S) with respect to the conductivity of the pore water σ_f while the diffuse layer is responsible for the excess surface conductivity Σ^d. The Stern layer is comprised between the o-plane (mineral surface) and the d-plane, which is the inner plane of the electrical diffuse layer. The diffuse layer extends from the d-plane into the pores.

Note that we have not made any assumption regarding the size of the diffuse layer. Usually, the thickness of the electrical double layer remains thin with respect to the size of the throats and the size of the grains. To the contrary of what we can find in the geophysical literature, the importance of surface conductivity has nothing to do with the ratio of the thickness of the diffuse layer with respect to the radius of the pores.

It should also be mentioned that the sorption of the counterions in the Stern layer can occur at different distances from the o-plane of Fig. 1 depending on the affinity of the counterions with the mineral silanol and aluminol surface sites, for instance. If the counterions keep their hydration shell, their mobility is likely to be close to their mobility in the free water. This is usually the case for sodium on silica. At the opposite, if the counterions are located close to the mineral surface, their mobility is likely to be much smaller than in the free water. This is the case of aluminium on silica, for instance. While not shown in this paper, this has dramatic implications regarding the spectral induced polarization signature of the sorption of cupper, zinc, or lead occurring on a mineral surface (P. Vaudelet, personal communication, 2009).

Surface conductivity corresponds to the electrical conduction in the electrical double layer coating the surface of the grains (e.g. Zukoski & Saville 1986a,b; Lyklema 1995, 2002; Revil & Leroy 2001). Apparently, two contributions can therefore co-exist. The first is the electrical conduction in the diffuse layer and the second is the electrical contribution of the Stern layer as described for instance in the dynamic Stern layer model of Zukoski & Saville (1986a). We denote g as the fraction of surface conductivity due to

the diffuse layer. This new partition coefficient is defined by

$$g = \frac{\sum_{i=1}^{Q} \beta_i^S |q_i| \Gamma_i^S}{\sum_{i=1}^{Q} \beta_i^S |q_i| \Gamma_i^S + \sum_{i=1}^{Q} \beta_i^d |q_i| \Gamma_i^d}, \tag{4}$$

where β_i^S and β_i^d are the mobilities of species i (expressed in m^2 s^{-1} V^{-1}) in the Stern layer and in the diffuse layer, respectively. Following Dukhin & Shilov (2002), Lyklema (2002), Tarasov & Titov (2007), and Leroy *et al.* (2008), we assume $\beta_i^S = \beta_i^d = \beta_i$ where β_i is the mobility of species i in the free water. This strong assumption is however not shared by Zukoski & Saville (1986b), for instance, and should be considered with caution.

We assume below a simple 1:1 salt completely dissociated electrolyte like NaCl. With these two assumptions, $f = g$, but we should keep in mind that this is not necessarily true for multicomponent electrolytes. The case of a multicomponent electrolyte will be discussed briefly later. In Fig. 2, we plot the value of $f = g$ for both various clay minerals and silica using the double layer models developed by Leroy *et al.* (2008) and Leroy & Revil (2009). We see that the value of f is very high for clays, which means that most of the counterions are located in the Stern layer. For both clays and silica, f increases with the salinity.

We assume now that there is no electrical conductivity contribution from the Stern layer at zero frequency (see Leroy *et al.* 2008). A simple equation to describe the DC electrical conductivity of a
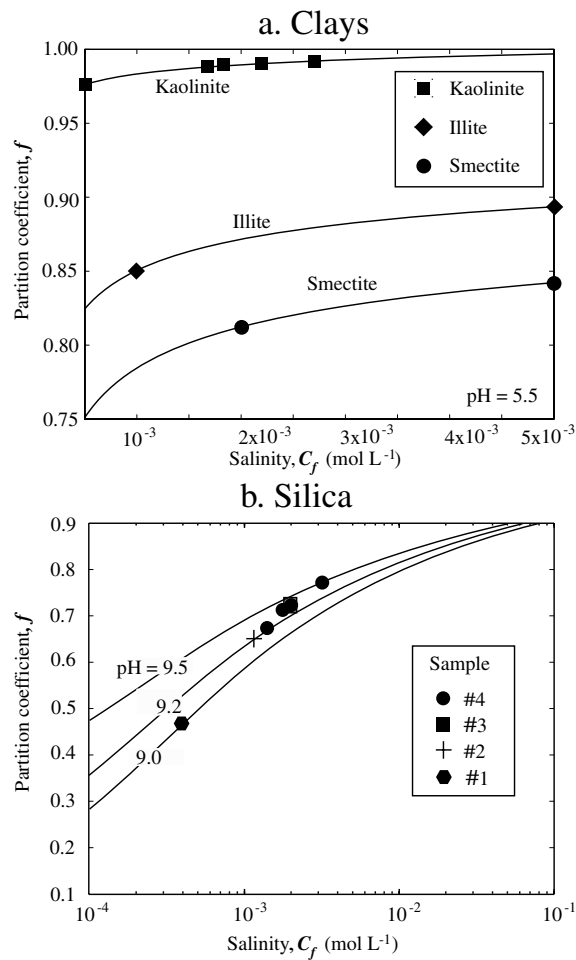
a. Clays

b. Silica

Figure 2. Comparison between the value of the partition coefficient for clay minerals and silica (modified from Leroy & Revil 2009). (a) Clay minerals. (b) Silica beads. The plain lines represent estimate from a triple layer model while the symbols are estimates from spectral induced polarization measurements as discussed by Leroy et al. (2008).

porous rock is given by having the pore space and surface conductivity working in parallel. The conductivity of the pore water is σ_f and the surface conductivity is the product of the charge concentration by the mobility of the counterions $\beta_{(+)}\bar{Q}_V$. These two contributions need to be divided by the formation factor to account for the tortuous paths of the current lines through the connected porosity. This yields

$$\sigma_0 = \frac{1}{F}(\sigma_f + \beta_{(+)}\bar{Q}_V). \tag{5}$$

We replace now the volumetric charge density of the diffuse layer per unit pore volume $\bar{Q}_V$ using eq. (2). This yields

$$\sigma_0 = \frac{1}{F}[\sigma_f + \beta_{(+)}(1-f)Q_V]. \tag{6}$$

We replace the quantity $\beta_{(+)}(1 - f)$ by an apparent mobility β_S. This gives

$$\sigma_0 = \frac{1}{F}[\sigma_f + \beta_S Q_V]. \tag{7}$$

Eq. (7) is derived in Appendix A from a different approach. This equation is also similar to the Waxman & Smits (1968) equation widely used in the oil industry to interpret borehole resistivity data.

However, in Waxman & Smits (1968), the non-linear behaviour of the conductivity curve (when plotted as a function of the conductivity of the brine) is described by using a non-physical dependence between the apparent mobility of the counterions and the salinity. Therefore, the apparent mobility of the counterions β_S in the models developed by Waxman & Smits (1968) and later by Revil et al. (1998, 2002), Revil & Glover (1998) and Revil (1999) should be understood as an apparent mobility of the counterions of the diffuse layer and not as a true mobility of the counterions in the Stern layer. The fact that the apparent mobility of the counterions is found to be 10 times smaller than the mobility of the same ions in the bulk pore water is actually coming from the partition of the charge between the Stern and the diffuse layers that should be accounted for in the conductivity model.

A last comment needs to be made before extending eq. (7) in the frequency domain. We point out that the linear conductivity model described above contradicts usually experimental data, which show that, at low salinities, the electrical conductivity of the porous material $\sigma_0(\sigma_f)$ is a non-linear function of the conductivity of the brine σ_f. Usually this observation is very well reproduced by conductivity models derived from the effective medium theory (see Bussian 1983; de Lima & Sharma 1992; Revil et al. 1998 for instance). This is because effective differential models use a distinct tortuosity for the bulk conductivity and for surface conductivity. Using such a non-linear model is avoided below because it is difficult to separate real and imaginary components analytically while this is very easy with a linear model. This is why in this paper, we will use a linear conductivity model. This assumption may be responsible for some of the bias observed below between the theory and the experimental data. However, obtaining a complete analytical model is a good start to go further in the near future towards a complete numerical or semi-analytical model using a non-linear conductivity model.

2.2 Permeability from surface conductivity

Using a perturbation theory of the DC-conductivity response of an uncharged porous material saturated by a brine, Johnson et al. (1987) obtained the following high salinity asymptote for the DC electrical conductivity of a saturated porous material with a diffuse layer coating the solid phase,

$$\sigma_0 = \frac{\sigma_f}{F}\left(1 + \frac{2}{\Lambda}\frac{\Sigma^d}{\sigma_f} + ...\right), \tag{8}$$

to the first order in the dimensionless parameter $\theta = 2\Sigma^d/\Lambda\sigma_f$ where Λ (in m) is the characteristic pore size of the porous material, Σ^d (in S) is the specific surface conductivity of the electrical diffuse layer (the excess electrical conductivity in the electrical diffuse layer with respect to the undisturbed pore water integrated over the thickness of the electrical diffuse layer, see Fig. 1). Eq. (8) can be also obtained using a volume-averaging approach of the local Nernst–Planck equation assuming a thin electrical double layer with respect to the two main radii of curvature of the mineral/pore water interface (Pride 1994) or by upscaling Joule dissipation (Bernabé & Revil 1995; Revil & Glover 1997). Eq. (8) is in principle valid for any type of pore space topology (including silica grains with clays lining, bridging, or filling the pores) as long as the pores are interconnected and the roughness of the mineral/pore water interface is not too severe.

Using a more specific approach (namely the effective differential medium theory for a granular material), Bussian (1983) and

De Lima & Sharma (1992) found the following high salinity asymptote

$$\sigma_0 = \frac{\sigma_f}{F} \left[1 + m(F-1) \frac{\sigma_S^0}{\sigma_f} + \cdots \right], \tag{9}$$

$$\sigma_S^0 = \frac{4\Sigma^d}{d_0}, \tag{10}$$

$$F = \phi^{-m}, \tag{11}$$

where σ_S^0 is the DC electrical conductivity of the solid grains, which is related to the specific surface conductivity of the electrical diffuse layer Σ^d and to the grain diameter d_0 by eq. (10). Eq. (11) represents Archie's law (Archie 1942) and m is called the first Archie exponent or the cementation exponent. Note that eq. (9) is consistent with eq. (A4) of Appendix A in the case where $m = 1$ in the pre-factor of the term $(1 - F)$. The conductivity of the grains is due to the electrical double layer coating the insulating grains (Fig. 1). Eq. (10) implies also that if all the grains have the same grain diameter d_0, they all have the same equivalent conductivity σ_S.

A comparison between eqs (8) and (9) yields an expression of the hydraulic pore radius Λ for a granular material as discussed by Revil & Cathles (1999)

$$\frac{1}{\Lambda} = \frac{2m(F-1)}{d_0}. \tag{12}$$

Despite the fact that eq. (12) is derived from high-salinity asymptotic behaviours, this relationship is independent of the salinity because it comprises only textural parameters.

The permeability k (in m^2) is related to F and Λ by (Johnson *et al.* 1986; Avellaneda & Torquato 1991; Bernabé & Revil 1995)

$$k = \frac{\Lambda^2}{8F}. \tag{13}$$

This relationship is very general and holds for a wide range of pore space topologies including the presence of cracks and clay habits in pores. However, in the following, we restrict our analysis to granular media. Combining eqs (12) and (13), the permeability of a granular material is given by (Revil & Cathles 1999; Revil 2007)

$$k = \frac{d_0^2}{32m^2(F-1)^2F}. \tag{14}$$

Revil & Cathles (1999) showed that eq. (14) works much better than the Kozeny–Carman equation to predict the permeability of consolidated and unconsolidated materials over a wide range of porosities. While derived using high salinity asymptotic behaviours for the electrical conductivity versus the salinity, eq. (14) is totally independent on the salinity as it involves only microgeometrical parameters.

2.3 Connection to induced polarization

Eq. (7) is a DC-conductivity equation. It needs to be generalized to AC-current conditions. In spectral induced polarization, one records the conductivity (or resistivity) from the magnitude of the current and the measured voltage (corrected by a geometrical factor depending on the position of the electrodes) and a phase between the AC-current and the voltage in response to a periodic AC-current. We note $\omega = 2\pi f$, the angular frequency, in rad s^{-1}, f is the frequency in Hz, and $i = (-1)^{1/2}$. The results can be written into a
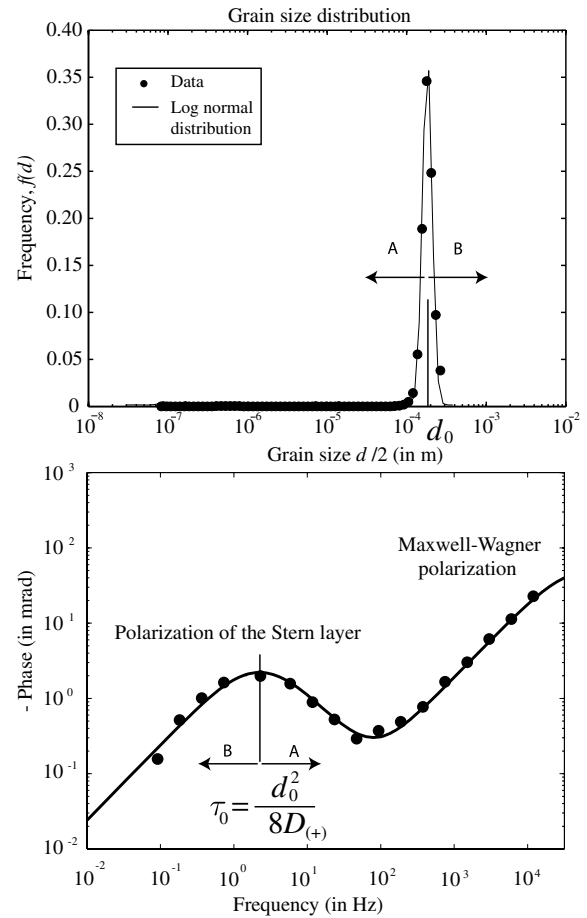

Figure 3. Phase as a function of the frequency for a granular material characterized by a log normal distribution (top panel). The tangent of the phase is defined as the imaginary part of the complex conductivity divided by the real part. Only the low frequency polarization results from the polarization of the Stern layer (see Leroy *et al.* 2008). When the grain size decreases (direction A), the relaxation frequency increases.

complex conductivity σ^*, a complex resistivity ρ^*, or a complex permittivity ε^* by

$$\sigma^* = \frac{1}{\rho^*} = i\omega\varepsilon^*. \tag{15}$$

In the following, we will work only with the complex conductivity. The relationship between the modulus of this conductivity $|\sigma|$ and the phase φ on one end and the real and imaginary components of the conductivity, σ' and σ, on the other, are given by

$$\sigma^* = |\sigma| \exp(i\varphi) = \sigma' + i\sigma'', \tag{16}$$

$$|\sigma| = \sqrt{\sigma'^2 + \sigma''^2}, \tag{17}$$

$$\tan\varphi = \sigma''/\sigma'. \tag{18}$$

A typical plot of the phase versus the frequency is given in Fig. 3. In the following we consider only low frequencies for which the spectral induced polarization results mainly from the polarization of the Stern layer and not from the Maxwell–Wagner polarization (see Fig. 3 showing relaxations associated with both the Stern layer
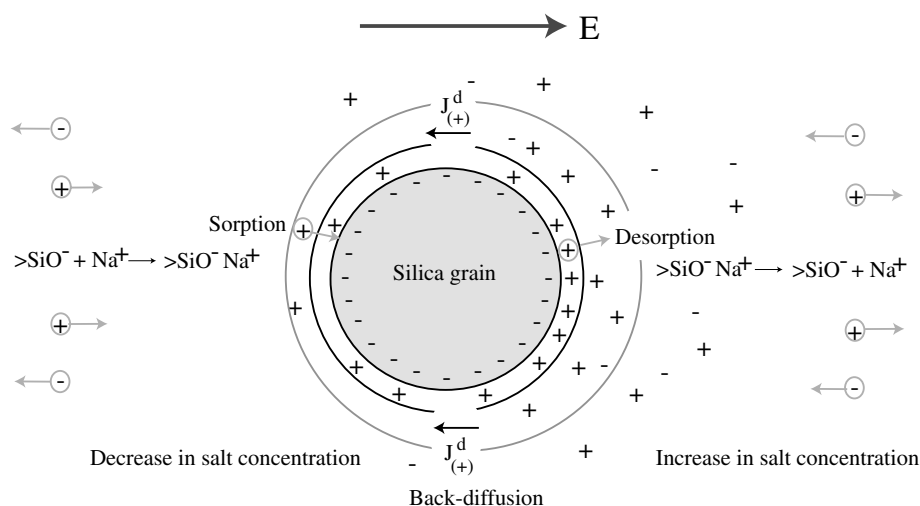
Figure 4. The presence of an applied electrical field **E** creates a dipole moment associated with the transfer of the counterions in both the Stern and the diffuse layers around a silica grain. This dipole moment points in the direction that is opposite to the applied field. The charge attached to the mineral framework remains fixed. The movement of the counterions in the Stern layer is mainly tangential along the surface of the grain. However, sorption and desorption of the counterions are in principle possible but they take time (typically a few hours). Back-diffusion of the counterions can occur both in the Stern and diffuse layers, and diffusion of the salt occurs in the pore space. In both cases, the diffusion of the counterions occurs over a distance that is equal to the diameter of the grains.

and the Maxwell–Wagner polarization). This assumption imposes a limitation in the grain size that can be investigated by induced polarization. Indeed, the polarization of the Stern layer of very small grains may occur at relatively high frequencies for which the Maxwell–Wagner polarization is the dominant mechanism of polarization (see Lesmes & Morgan 2001).

With these assumptions, we use the following complex surface conductivity model (De Lima & Sharma 1992, their eq. (6); Leroy *et al.* 2008; Leroy & Revil 2009):

$$\sigma_S = \frac{4}{d_0}(\Sigma^d + \Sigma^S) - \frac{4}{d_0}\frac{\Sigma^S}{1 + i\omega\tau_0}. \tag{19}$$

$$\tau_0 = \frac{d_0^2}{8D_i}, \tag{20}$$

where Σ^d is the specific surface conductivity associated with the diffuse layer and Σ^S is the specific surface conductivity associated with the Stern layer at high frequencies $\omega \gg 1/\tau_0$ and D_i is the diffusion coefficient of species *i*. Eq. (19) unifies the theories of O'Konski (1960) and Schwarz (1962) as done by Schurr (1964). In the model of O'Konski, the surface conductivity is frequency-independent and its influence upon the Maxwell–Wagner polarization of an assemblage of particles is investigated. Schwarz (1962) developed a frequency-dependent surface conductivity model for a compact layer of counterions surrounding the grains with the counterions moving only along the mineral surface.

The real situation is more complicated, as illustrated in Figs 4 and 5. The presence of an electrical field displaces the electrical diffuse layer in the case where there is no overlap in the diffuse layer (so only in the dilute suspension of sphere in a background electrolyte). The total current entering the left-hand side of Fig. 4 flows in the background electrolyte. In the centre part of the figure and at high values of the Dukhin number, the current is mainly restricted to the electrical double layer. Because the counterions are usually located in the Stern layer (Section 2.1), most of the current is located in the Stern layer. In steady-state conditions, these currents must have the same magnitude. The electrical current transported

by counterions and coions is proportional to their concentrations but there is mainly counterions in the electrical double layer. The coions cannot penetrate the double layer because of Coulombic repulsion. Consequently, in the centre part of Fig. 4, the fraction of the total current carried by the coions and the counterions, the so-called Hittorf numbers (Revil 1999), is different in the bulk electrolyte and in the electrical double layer. At the opposite, the flow of counterions entering the left-hand side of the figure is the same as the flow of coions leaving this side of the figure. Therefore the number of counterions arriving per unit time towards the left-hand side of the grain is smaller than the number of counterions transferred in the electrical double layer. There is therefore a depletion of the counterions on the left-hand side of the grain. At the opposite, the number of coions coming to the right-hand side of the figure cannot be all transferred on the left-hand side. So they accumulate on the right-hand side of the grain. As the result, there is an increase of the salinity to the right-hand side of the grain and a depletion in the salt concentration on the left-hand side of the grain. In this case, there is a back-diffusion through the pore space of the material and the diffusion coefficient is the mutual diffusion coefficient of the salt through the pore space (Revil 1999). This mechanism is called membrane polarization in the literature (Vinegar & Waxman 1974).

However, there is also the possibility that the back-diffusion occurs in the Stern layer itself and in this case, the diffusion coefficient entering into the relaxation time is the diffusion coefficient of the counterions in the Stern layer. This diffusion coefficient can be related to the mobility of the counterions in the Stern layer by the Nernst–Einstein relationship, $D_i = k_b T \beta_i/|q_i|$ where k_b is the Boltzmann constant (1.3807×10^{-23} J K^{-1}), T is the absolute temperature, and $|q_i|$ is the absolute value of the charge of the counterions in the Stern layer. According to the dynamic Stern layer model of Zukoski & Saville (1986a), diffusion of the counterions along the Stern layer is possible and therefore we will favour the first assumption in this paper.

The increase of the ion concentration on one side of the pores is responsible for the membrane polarization also widely described in the literature (e.g. Marshall & Madden 1959; Titov *et al.* 2002). A
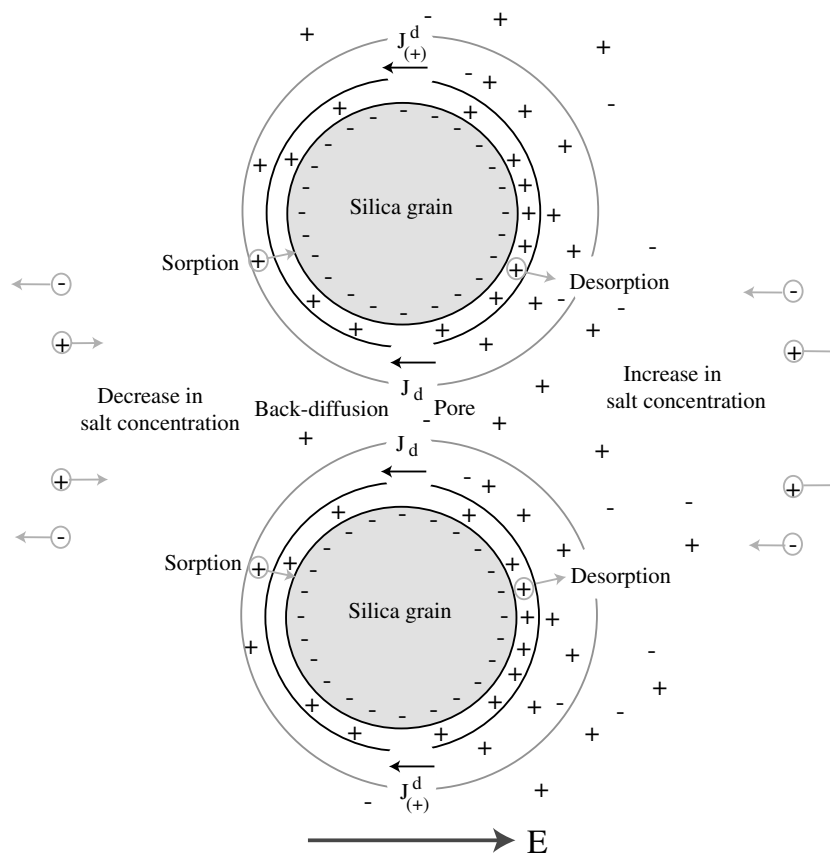
Figure 5. Sketch of membrane polarization of a pore sandwiched between two grains. The back-diffusion can occur both in the electrical double layer for the counterions and in the bulk pore water for the coions. The salt accumulated on one side of the pore diffuses back with a diffusion coefficient that is equal to the mutual diffusion coefficient of the salt (see Revil, 1999 for an expression of the mutual diffusion coefficient).

sketch of the build-up of salinity gradient across a pore sandwiched between two grains is shown in Fig. 5. In this case, the length scale of polarization is again the diameter of the grain. At high frequencies there is no time for the diffusion to take place while diffusion redistributes the charge carriers at low frequencies.

Another point concerns the anisotropy of the complex surface conductivity in the Stern layer. In the model of Schwarz, the surface conductivity of the Stern layer is anisotropic as the counterions cannot leave the Stern layer. At the opposite, some models introduce both normal and tangential components of the specific surface conductivity of the Stern layer (see for instance Chassagne *et al.* 2002). Usually the kinetic of the sorption/desorption of the counterions in the Stern layer is a slow process that can take several hours to reach equilibrium. Therefore, we favour in this paper a model in which the counterions can only move tangentially along the mineral/water interface.

De Lima & Sharma (1992) used eq. (19) to investigate the polarization of the electrical double layer with the frequency-independent contribution associated with the diffuse layer and the frequency-dependent contribution associated with the Stern layer. However, they favour in their paper another model of polarization of the diffuse layer, namely the Fixman's model developed initially to model the polarization of suspensions of colloids, each colloidal particle being surrounded by a diffuse layer of counterions responsible for a strong polarization of the colloidal suspension at low frequencies (Fixman 1980). Because the diffuse layer of a dense aggregate of grains is continuous, we doubt that there is a charge accumulation

associated with the polarization of the diffuse layer and we dismiss this contribution in our model.

A description of the two contributions to the specific surface conductivity (sometimes called the specific surface conductance because it is expressed in Siemens) is sketched in Fig. 1. Eq. (19) represents the conductivity of an insulating sphere coated with the electrical double layer with the following assumptions. (1) The double layer is thin with respect to the radius of the grains. (2) The charges of the Stern layer can move only tangentially along the mineral surface. Back-diffusion in the Stern layer is responsible for the decay of this contribution with the decrease of the frequency. (3) The polarization of the diffuse layer is minimized by the fact that the diffuse layer is above a percolation threshold at the scale of a representative elementary volume. Therefore there is no or only small deformation of the diffuse layer in response to an electrical field.

The relaxation time τ_0 is the time required to establish a stationary ionic distribution in the Stern layer coating a grain of diameter d_0 under the action of a static electrical field. Eq. (20) implies that the relaxation time scales with the square of the grain size, a result confirmed for instance in the laboratory by Titov *et al.* (2002) using sieved sands and by Leroy *et al.* (2008) using glass beads as well as in colloidal chemistry (Swan 2000).

We define a low-frequency and high-frequency asymptotic surface conductivities as

$$\sigma_S^0 = \frac{4}{d_0} \Sigma^d, \tag{21}$$

$$\sigma_S^\infty = \frac{4}{d_0}(\Sigma^d + \Sigma^S). \tag{22}$$

With these definitions, we can write eq. (19) as

$$\sigma_S = \sigma_S^\infty + \frac{\sigma_S^0 - \sigma_S^\infty}{1 + i\omega\tau_0}. \tag{23}$$

According to this model, surface conductivity is characterized by a low-frequency asymptotic value, σ_S^0, and a high-frequency asymptotic value, σ_S^∞. The transition between both values occurs at frequencies corresponding to the inverse of the relaxation time τ_0. This case corresponds to the case of a Dirac distribution for the relaxation time. Replacing the grain diameter in eq. (14) by the expression of the relaxation time, eq. (20), we obtain the following equation for the permeability as a function of the relaxation time

$$k = \frac{D_i \tau_0}{4m^2(F-1)^2 F}. \tag{24}$$

In this equation, the permeability depends linearly on the relaxation time.

In previous approaches found in the literature, the exponents between the permeability and the formation factor and between the permeability and the main relaxation time were fitted according to the data using a general empirical relationship written as $k = a\tau_0^b F^c$ where a, b and c were fitting constants. These constants were not predicted from the theory. In our model, we predict the values of a, b and c.

We first perform a comparison between the prediction of eq. (24) and the data reported in Tong *et al.* (2006b, table 1) who used time domain induced polarization to extract the main relaxation time τ_0 stating that the relaxation curve can be described by a sum of decreasing exponentials (this idea can be traced back to Wagner 1914). They investigated 123 clayey sandstone core samples from the Daqing oil field in China. These samples were saturated by a 5 g L^{-1} NaCl solution ($D_{Na+} = 1.29 \times 10^{-9}$ m^2 s^{-1}). They also measured the permeability (with gas) and found that the permeability was in the range 0.1–770 mD and the porosity was in the range 0.071 and 0.215. A comparison between the prediction of eq. (24) and their data is shown in Fig. 6. Despite the fact that the formation factors were measured, their values were not reported by Tong *et al.* (2006b). In our evaluation, the formation factors were computed from the porosities using Archie's law, eq. (11), with $m = 2$ as default value (classical Archie's law is indeed $F = \phi^{-2}$). A comparison between the measured and predicted permeabilities is reported in Fig. 6. We obtain a fair comparison between the model and the data without the use of any flush factor. This is however a substantial improvement over the method proposed by Tong *et al.* (2006b), which requires a formation-dependent fit of the data.

We consider next the case of an unconsolidated sand or a pack of glass beads. Taking $m = 3/2$ (the value of the cementation exponent for a pack of spherical grains according to the differential effective medium theory, see Sen *et al.* 1981) and $F >> 1$, we obtain

$$k = \frac{D_i \tau_0}{9F^3}. \tag{25}$$

This equation is consistent to eq. (2.40) from Kemna (2000, p. 34) who suggested that the permeability is proportional to τ_0/F^u with the exponent u depending on both the cementation exponent m and the fractal dimension of the pore/mineral interface.

A number of measurements have been performed with sands. For cohesionless sands, usually $m = 1.3$ (Sen *et al.* 1981; Börner *et al.* 1996) and the porosity of a random packing of sphere is typically 0.36. This yields $F^3 = 54$. Taking $D_i = 2.45 \times 10^{-9}$ m^2 s^{-1}
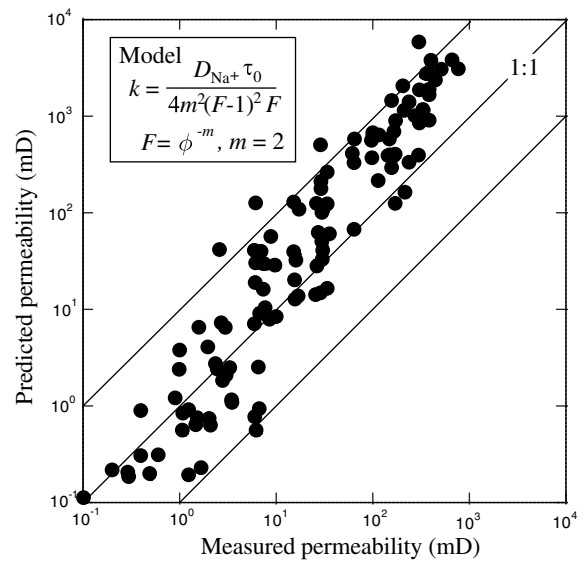
Figure 6. Comparison between the simplified model developed in Section 2 and the data (relation time from time domain induced polarization and measured gas permeability) from Tong *et al.* (2006b, their table 1). We see that the predictions are accurate inside one order of magnitude over four decades without the need for free-parameters. The two solid lines parallel to the 1:1 line correspond to a variation of plus or minus one order of magnitude with respect to the predicted trend.

as proposed by Leroy *et al.* (2008) for their pore water composition (see their table 2), we obtain $k \approx a\tau_0$ with $a = 5 \times 10^{-12}$ m^2 s^{-1}. This is can be compared to the data reported by Kemna *et al.* (2005) who found $k \approx a\tau_0^b$ with $a = 3.8 \times 10^{-12}$ m^{2}s^{-1} and $b = 0.56$. We believe that the discrepancy between the model prediction and the experimental data results from the inability of the equations derived above to account well for the true grain size distribution or/and the possibility of an additional contribution like membrane polarization (Vinegar & Waxman 1984).

We apply now our model to the data of Scott & Barker (2003). These authors performed spectral induced polarization measurements using Permo-Triassic sandstones with pore lining clays and oxyhydroxides. They noted a strong correlation from the pore throat diameter of their samples, determined from mercury injection measurements, and the main relaxation frequency exhibited by the phase in the frequency band 1 mHz – 1 kHz. According to them, this was suggesting that the polarization process responsible for this correlation was occurring in the pore space (possibly involving a membrane polarization mechanism) and not along the pores. We consider that the main relaxation frequency is given by $f_0 = 1/(2\pi \tau_0)$. Considering eqs (12) and (20), the pore diameter is given by

$$2\Lambda = \frac{\sqrt{8D_i/2\pi}}{m(F-1)} \frac{1}{\sqrt{f_0}}. \tag{26}$$

The porosity is in the interval 0.124–0.324, which with $m = 2$ (the default value of the cementation exponent for sandstone, see Waxman & Smits 1968; Revil *et al.* 1998 for instance) yields $10 < F < 65$. Therefore, $18 < m(F - 1) < 128$. We take $D_i = 2 \times 10^{-9}$ m^2 s^{-1} as default value as explained above. A comparison between the model estimates using the bounds derived above for the formation factor and the experimental data of Scott & Barker (2003) is shown in Fig. 7. The bounds determined with our model agree with the data for which the bounds the pore diameter was independently determined by mercury intrusion measurements.
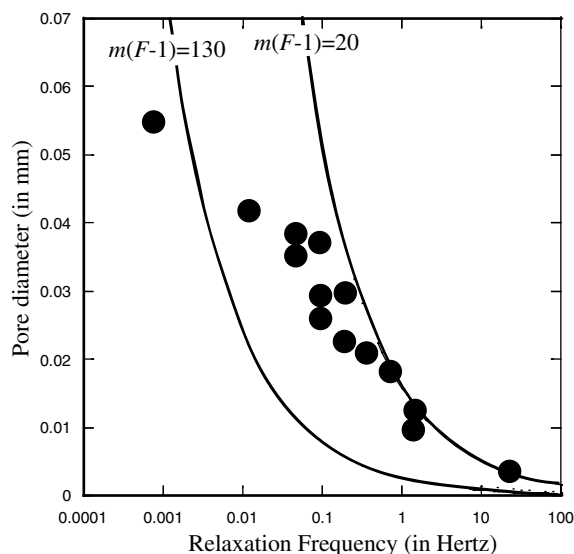
Figure 7. Pore diameter as a function of the relaxation frequency. The two lines are the envelope of our model for the two extreme estimates of the formation factor. The black circles are the data points from Scott & Barker (2003). The uncertainty in the measurements is roughly equal to the size of the symbols. Note that all the data except one are contained between our bounds described by the two solid lines.
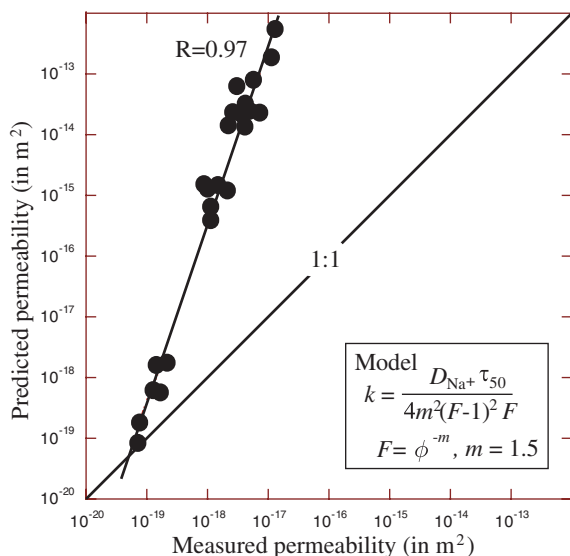

Figure 8. Application of the permeability formula developed in the main text for the case corresponding to a delta function in the particle size distribution as a function of the measured permeability for a material characterized by a broad range of grain size. Data from Zisser *et al.* (2009) used with permission from the authors.

Another test we performed in this section concerns the data of Zisser *et al.* (2009) performed on tight gas sandstone. This sandstone is characterized by relatively broad grain size distribution. Zisser *et al.* (2009) inverted the distribution of relaxation time (see next section). From this distribution, they determined the relaxation time τ_{50}, which is the relaxation time at which 50 per cent of the relaxation times in the distribution is smaller. Application of eq. (24) to their datasets using τ_{50} as a proxy for τ_0 is shown in Fig. 8. We see that there is a very strong correlation between the predicted permeability and the measured permeability ($R = 0.97$). However the slope is not correctly predicted. In turn this means that τ_{50} is
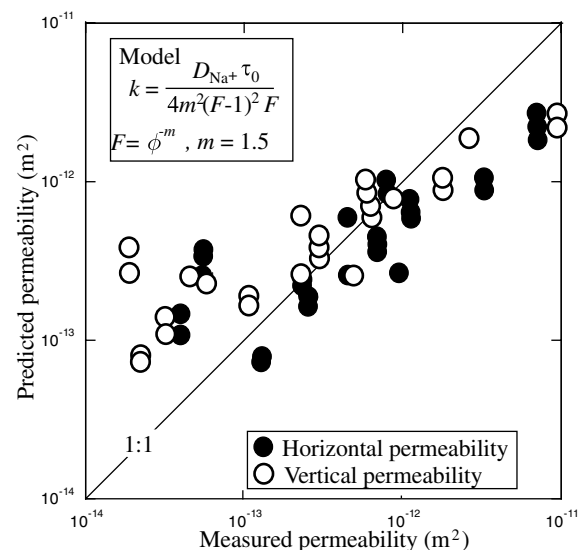

Figure 9. Comparison between the simplified model developed in Section 2 and the data from Binley *et al.* (2005) ($R = 0.93$).

not the relevant characteristic time to compute permeability when the distribution of grain size is broad.

The last test is performed with the data from Binley *et al.* (2005). They use core samples from the UK Triassic sandstone aquifer from Eggborough and Hatfield. They performed the following measurements (1) grain size distribution, (2) scanning electron microscope (SEM) imaging and analysis to determine sample composition, (3) mercury injection capillary pressure tests to determine pore throat size distributions and total porosity, (4) gas permeability, (5) cation exchange capacity (CEC) and (6) pore surface area on intact sub-samples using nitrogen gas adsorption. For their spectral induced polarization measurements, the samples were saturated with a pore water solution at 0.10 S m^{-1} (at 25 °C) with the following concentrations in ionic species: $C(Cl^-) = 0.9$ Mol L^{-1}, $C(NO_3^-) = 11.4$ Mol L^{-1}, $C(SO_4^-) = 0.9$ Mol L^{-1}, $C(Na^+) = 0.9$ Mol L^{-1}, $C(Mg^{2+}) = 0.9$ Mol L^{-1}, and $C(Ca^{2+}) = 5.7$ Mol L^{-1}. The permeability is computed with eq. (24) with $D_i = 2.45 \times 10^{-9}$ m^2 s^{-1} as proposed by Leroy *et al.* (2008). The formation factors are determined from Archie's law with $m = 1.5$, which is suitable for weakly consolidated sandstone (see above). The comparison between the predicted and measured permeabilities is shown in Fig. 9 and is fair.

3 GENERALIZATION

Real granular media are characterized by a grain size distribution and therefore by a distribution of the relaxation times. However, few works have considered the effect of the grain size distribution upon induced polarization. Carrique *et al.* (1998) performed a numerical study of the effect of the polydispersity of suspensions of spherical particles on their dielectric behaviour, in both the frequency and time domains, using the model proposed by DeLacey & White for monodisperse suspensions. They found that both in the frequency and time domains the predicted behaviour does not differ in any essential way from the one obtained for a monodisperse suspension with particle radius close to the volume-averaged mean radius of the polydisperse system. However, they used a very narrow particle size distribution that was Gaussian distributed.

Starting with the models of Fixman and Schwarz, Lesmes & Morgan (2001) investigated the role of the particle size distribution of a sandstone upon induced polarization. They found that the particle size distribution is of paramount importance to model the low-frequency electrical conductivity of rocks. In the following, we follow their idea and we develop new expressions to incorporate the particle size distribution. We will also extend the relationship developed in Section 2 to estimate permeability to a granular material with an arbitrary grain size distribution.

3.1 The distribution of relaxation times

We consider below the case of a granular material characterized by a grain size distribution $f(D)$ where D is a given grain diameter. In addition, we consider that grains of different mineralogy have very similar surface conductance, an assumption that is in good agreement with various experimental data (see Revil *et al.* 1999; Leroy & Revil 2004). The case discussed in Section 2 above corresponds to $f(D) = \delta(D - d_0)$ where δ corresponds to the Dirac distribution. This grain size distribution is associated with a distribution of relaxation times $g(\tau)$. Using the superposition principle, the surface conductivity is given by:

$$\sigma_S = \sigma_S^\infty + \left(\sigma_S^0 - \sigma_S^\infty\right) \int_0^\infty \frac{g(\tau)}{1 + i\omega\tau} d\tau, \tag{27}$$

$$\int_0^\infty g(\tau) d\tau = 1. \tag{28}$$

The integral on the right-hand side of eq. (27) is called the reduced polarization by Fuoss & Kirwood (1941) and the spectral shape function by Yeung & Shin (1991). If $g(\tau)$ reduces to a Dirac distribution, $g(\tau) = \delta(\tau - \tau_0)$, eq. (27) reduces to the Debye distribution analysed in the previous section, eq. (23).

Eq. (27) means that there is a low-frequency and a high-frequency value of surface conductivity. The low-frequency value of surface conductivity is associated with the diffuse layer. This low-frequency conductivity response should be convoluted by a grain size distribution. The high-frequency value of surface conductivity results both from the diffuse and Stern layer conductivities and should be also convoluted by a grain size distribution as shown below. The transition between low frequencies to high frequencies is not characterized by a single relaxation time but by the distribution of relaxation times $g(\tau)$ (Lesmes & Morgan 2001).

We are looking now for a relationship between the distributions $g(\tau)$ and $f(D)$. The real and imaginary parts of surface conductivity of the grains are obtained by the following expressions:

$$\sigma_S' = \sigma_S^\infty + \left(\sigma_S^0 - \sigma_S^\infty\right) \int_0^\infty \frac{g(\tau)}{1 + \omega^2\tau^2} d\tau, \tag{29}$$

$$\sigma_S'' = -\left(\sigma_S^0 - \sigma_S^\infty\right) \omega \int_0^\infty \frac{g(\tau)\tau}{1 + \omega^2\tau^2} d\tau. \tag{30}$$

We consider that the grain diameter distribution $f(D)$ is normalized,

$$\int_0^\infty f(D) dD = 1. \tag{31}$$

We note as $h(\eta)$ the normalized distribution of the inverse of the grain diameters, with η being the inverse of the grain diameter $\eta = 1/D$. The two probability density functions $f(D)$ and $h(\eta)$ are related to each other by their probability distributions,

$$h(\eta) |d\eta| = f(D) dD. \tag{32}$$

Eq. (32) means that the probability distribution to find the inverse of the grain size between η and $\eta + d\eta$ is the same as finding the grain size between D and $D + dD$. Using $|d\eta| = (1/D^2) dD$, we obtain

$$h(\eta) = D^2 f(D). \tag{33}$$

We apply now the superposition principle to eq. (19),

$$\sigma_S = 4 \int_0^\infty h(\eta)\eta \left[\left(\Sigma^d + \Sigma^S\right) - \frac{\Sigma^S}{1 + i\omega\tau} \right] d\eta, \tag{34}$$

We can replace $h(\eta)\eta d\eta$ by $f(D) d\ln D$. With $0 < D < +\infty$ (note that D is of course bounded by an upper value $D_{\max}$ that should be much smaller that the characteristic size of the representative elementary volume of the granular material that is considered here), we have $0 < \ln D < +\infty$. Therefore, we obtain

$$\sigma_S = 4 \int_0^{+\infty} f(D)(\Sigma^d + \Sigma^S) d\ln D$$
$$+ 4 \int_0^{+\infty} f(D) \left(\frac{\Sigma^S}{1 + i\omega\tau} \right) d\ln D. \tag{35}$$

As Σ^d and Σ^S characterize the local properties of the electrical double layer (Fig. 1), they are strictly independent of the grain size distribution so they can be move out from the two integrals. This yields

$$\sigma_S = 4(\Sigma^d + \Sigma^S) \int_0^{+\infty} f(D) d\ln D$$
$$+ 4\Sigma^S \int_0^{+\infty} f(D) \left(\frac{1}{1 + i\omega\tau} \right) d\ln D. \tag{36}$$

Therefore, the high and low frequencies asymptotic values of surface conductivities of the porous material are

$$\sigma_S^\infty = 4(\Sigma^d + \Sigma^S) \int_0^{+\infty} f(D) d\ln D, \tag{37}$$

$$\sigma_S^0 = 4\Sigma^d \int_0^{+\infty} f(D) d\ln D, \tag{38}$$

which generalize eqs (21) and (22). Eqs (37) and (38) show explicitly how the low-frequency and high-frequency asymptotic values of surface conductivity can be computed from the grain size distribution. From eqs (37) and (38), we have

$$\sigma_S^\infty - \sigma_S^0 = 4\Sigma^S \int_0^{+\infty} f(D) d\ln D, \tag{39}$$

and therefore

$$4\Sigma^S = \frac{\sigma_S^\infty - \sigma_S^0}{\int_0^{+\infty} f(D) d\ln D}. \tag{40}$$

Inserting eqs (37) and (40) into eq. (36) yields

$$\sigma_S = \sigma_S^\infty + \left(\sigma_S^\infty - \sigma_S^0\right) \frac{\int_0^{+\infty} f(D) \left(\frac{1}{1+i\omega\tau}\right) d\ln D}{\int_0^{+\infty} f(D) d\ln D}. \tag{41}$$

Comparing now eq. (41) with eq. (27) yields the following equality:

$$\int_0^\infty \frac{g(\tau)}{1 + i\omega\tau} d\tau = \frac{\int_0^{+\infty} \left(\frac{f(D)}{1+i\omega\tau}\right) d\ln D}{\int_0^{+\infty} f(D) d\ln D}, \tag{42}$$

and therefore this implies in turn

$$\frac{f(D) d\ln D}{E_h} = g(\tau) d\tau, \tag{43}$$

where E_h is the expected value of the probability density function $h(\eta)$ (see demonstration in Appendix B)

$$E_h = \int_0^{+\infty} f(D) \mathrm{d} \ln D. \tag{44}$$

Integrating eq. (43) over the full range of relaxation times and grain sizes is consistent with eq. (28) expressing that the distribution of the relaxation times is normalized. Taking also a delta distribution for the grain size distribution and for the distribution of the relaxation times is also consistent. The relationship between the relaxation time and the grain diameter is $\tau = D^2/8D_S$. Differentiating this equation yields

$$\mathrm{d}\tau = \frac{D \mathrm{d} D}{4 D_S}. \tag{45}$$

Inserting eq. (45) into eq. (43) and using $\tau = D^2/8D_S$, we obtain

$$\tau g(\tau) = \frac{f(D)}{2 E_h}. \tag{46}$$

We introduce the function

$$F(s) = \frac{f(d_0 \mathrm{e}^{s/2})}{\int_{-\infty}^{+\infty} f(d_0 \mathrm{e}^{s/2}) \mathrm{d} s}, \tag{47}$$

$$\int_{-\infty}^{+\infty} F(s) \mathrm{d} s = 1, \tag{48}$$

where the variable s is defined by

$$s = 2 \ln \left(\frac{D}{d_0} \right) = \ln \left(\frac{\tau}{\tau_0} \right), \tag{49}$$

$$\mathrm{d} s = 2 d \ln D = \mathrm{d} \ln \tau, \tag{50}$$

where d_0 is a characteristic grain size (e.g. the median of the grain size distribution) and τ_0 the associated relaxation time. Therefore we have

$$\tau g(\tau) = F(s), \tag{51}$$

and we check the property $g(\tau) \mathrm{d}\tau = F(s) \, \mathrm{d} s$, the probability to find the relaxation time between τ and $\tau + \mathrm{d}\tau$ is equal to the probability to find s between s and $s + \mathrm{d}s$. The function $F(s)$ describes the grain size distribution with respect to the log of the grain size. Eqs (47)–(51) provide relationships between the distribution of the relaxation times $g(\tau)$ and the distribution of the grain diameters $f(D)$. This is what we were looking for.

Cole & Cole (1941) and Fuoss & Kirwood (1941, their eq. 3) analysed in depth the special cases where $F(s)$ is a log normal distribution and a Cole–Cole distribution. These particular functions will be analysed in Section 3.4 because they have practical applications to interpret experimental data. Indeed, the grain size distribution is often described in the literature using a log normal distribution and the interpretation of induced polarization data is often performed with the Cole–Cole model. We believe that there is a direct connection here to look for.

3.2 A new equation for permeability

We are now ready to find a new equation for the permeability of a granular material defined by a given porosity and a grain size distribution. Using the analysis made in Section 2.2, eq. (12), we see that the transformation

$$\frac{1}{d_0} \to E_h \equiv \int_0^{+\infty} f(D) \mathrm{d} \ln D \tag{52}$$

implies that the length scale Λ can be generalized to give

$$\frac{1}{\Lambda} = 2m(F-1)E_h. \tag{53}$$

In addition, we consider that the formation factor and the cementation exponent are independent of the grain size distribution because they depend on the grain shape distribution and the porosity, for example, from differential effective medium theory or a volume average of the Nernst–Planck equation. Using eq. (53) in eq. (13) yields the following equation for the permeability:

$$k = \frac{1}{32 m^2 F(F-1)^2} E_h^{-2}, \tag{54}$$

$$k \approx \frac{1}{72 F^3} E_h^{-2}. \tag{55}$$

Note that in the case where the grain size distribution is given by the delta function $f(D) = \delta(D - d_0)$, we recover from eqs (53) and (55) the formula given in Section 2 for Λ and k. In the case of a broad distribution of relaxation times, more weight is given to the smallest grains in agreement with ideas expressed in the literature (see Berg 1970; Kemna 2000 and Appendix B).

3.3 Special cases

We consider now the special cases of the Cole–Cole and log normal probability distribution models (see for instance Cole & Cole (1941, their section VI-C) and De Mey 1974)

$$F(s)\mathrm{d}s = \frac{1}{2\pi} \frac{\sin[\pi(1-\alpha)]}{\cosh[\alpha s] - \cos[\pi(1-\alpha)]} \mathrm{d}s, \tag{56}$$

$$F(s)\mathrm{d}s = \frac{1}{\sqrt{2\pi}\hat{\sigma}} \exp\left[-\left(\frac{s}{\sqrt{2}\hat{\sigma}} \right)^2 \right] \mathrm{d}s, \tag{57}$$

where $s = 2 \ln(D/d_{50})$ (d_{50} represents the median of the grain size distribution), α is the Cole–Cole exponent ($0 \leq \alpha \leq 1$, $\alpha = 1$ corresponds to a Debye model), $\hat{\sigma}$ represents the standard deviation of the Gaussian distribution describing $F(s)$ in eq. (57). In these two cases, the grain size probability distributions are given by (see Appendix B),

$$f(D) = \frac{1}{\pi} \frac{\sin[\pi(\alpha-1)]}{\cosh[2\alpha \ln(D/d_{50})] - \cos[\pi(\alpha-1)]}, \tag{58}$$

$$f(D) = \frac{1}{D\sqrt{2\pi}\sigma} \exp\left[-\frac{(\ln D - \mu)^2}{2\sigma^2} \right], \tag{59}$$

where $\sigma = \hat{\sigma}/2$ and $\mu = \ln d_{50}$. Using eqs (51), (56) and (57), we get the probability distributions of the relaxation times (Appendix B)

$$g(\tau)\mathrm{d}\tau = \frac{1}{2\pi} \frac{\sin[\pi(\alpha-1)]}{\cosh[\alpha \ln(\tau/\tau_0)] - \cos[\pi(\alpha-1)]} \mathrm{d} \ln\left(\frac{\tau}{\tau_0} \right), \tag{60}$$

$$g(\tau)\mathrm{d}\tau = \frac{1}{\sqrt{2\pi}\hat{\sigma}} \exp\left[-\left(\frac{\ln(\tau/\tau_0)}{\sqrt{2}\hat{\sigma}} \right) \right] \mathrm{d} \ln\left(\frac{\tau}{\tau_0} \right). \tag{61}$$

The question we address below is why the Cole–Cole distribution fits well the experimental polarization spectra at low frequencies. As explained by Cole & Cole (1941), the log normal and the Cole–Cole probability distributions are quite similar when the Cole–Cole exponent α is between 0.5 and 1 (see their fig. 9). Sedimentary rocks

have grain size distributions usually described by one or the sum of two or three log normal distributions. It is therefore not surprising that the polarization spectra can be fitted by a Cole–Cole distribution or the sum of several Cole–Cole distributions. This explains also the success of the Cole–Cole distribution in solving a number of problems controlled by the grain size distribution like the deformation of silica aggregates by pervasive pressure solution at the grain-to-grain contacts (Revil *et al.* 2006). However, the particle size distribution of soils, for instance, has been also described by a fractal model (Posadas *et al.* 2001). This implies a very broad distribution of the relaxation time distribution of such soils that can be reproduced by the Cole–Cole model, which has tails that are much longer than the log normal distribution for the Cole–Cole exponent is comprised between 0 and 0.5.

Another reason for the success of the Cole–Cole model was noted by Swan (2000) for dielectric spectra. Swan noted that that circular plot in an Argand diagram are approximated by almost any logarithmic symmetrical distribution function like the log normal distribution. Differences appear only at frequencies well above or well below the relaxation frequency and these frequencies are generally not investigated, so data are usually missing to discriminate the Cole–Cole model from other logarithmic symmetrical functions.

This Cole–Cole distribution of relaxation times implies that surface conductivity is described by (see Cole & Cole 1941)

$$\sigma_S = \sigma_S^\infty + \left(\sigma_S^0 - \sigma_S^\infty\right)\left[\frac{1}{1 + (i\omega\tau)^\alpha}\right]. \tag{62}$$

We consider for simplicity a linear model,

$$\sigma^* = \frac{1}{F}[\sigma_f + (F-1)\sigma_S]. \tag{63}$$

Therefore, the overall conductivity model follows a Cole–Cole model,

$$\sigma^* = \sigma_\infty + \frac{\sigma_0 - \sigma_\infty}{1 + (i\omega\tau)^\alpha}, \tag{64}$$

$$\sigma_0 = \frac{1}{F}\left[\sigma_f + (F-1)\sigma_S^0\right], \tag{65}$$

$$\sigma_\infty = \frac{1}{F}\left[\sigma_f + (F-1)\sigma_S^\infty\right]. \tag{66}$$

Therefore, our analysis provides a theoretical foundation for the use of the Cole–Cole model to describe the low-frequency behaviour of the complex conductivity of granular media saturated by a brine. In addition, the partition coefficient described in Section 2 can be related to the high and low surface conductivities,

$$f = \frac{\Sigma^S}{\Sigma^S + \Sigma^d} = \frac{\sigma_S^\infty - \sigma_S^0}{\sigma_S^\infty}, \tag{67}$$

and therefore,

$$\sigma_\infty = \frac{1}{F}\left[\sigma_f + (F-1)\frac{\sigma_S^0}{1-f}\right]. \tag{68}$$

Because f can be computed from a double layer model (see Leroy *et al.* 2008 and Leroy & Revil 2009), the model has two unknowns only, F and σ_S^0, that can be determined from the low and high asymptotic values of the electrical conductivity. We can also compute the chargeability M as a function of f. The chargeability M is defined as

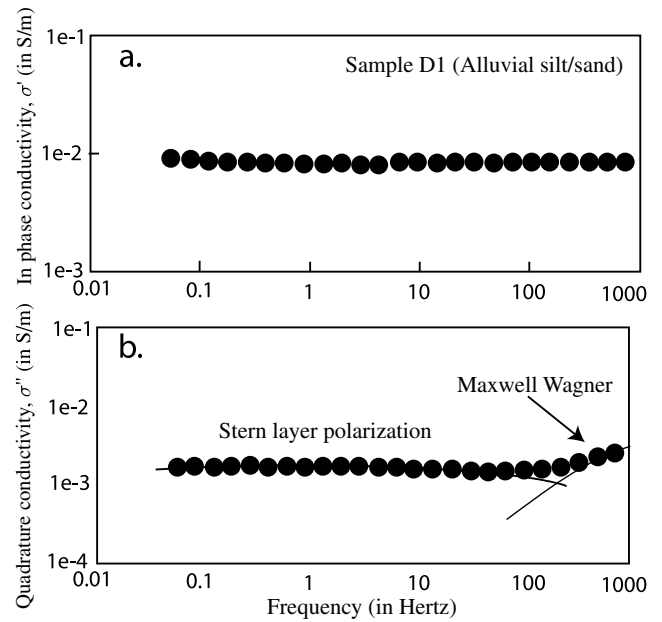$$M = 1 - \frac{\sigma_0}{\sigma_\infty}, \tag{69}$$

Figure 10. In phase and quadrature conductivity for a alluvium silt sand sample (sample D1 from Slater & Lesmes 2002b) characterized by a broad grain size distribution. Note the very flat quadrature conductivity (and therefore the phase) in the frequency range 0.01–100 Hz due to the broad grain size distribution. The lines are guides for the eyes. Usually this type of behaviour is modelled by a constant phase angle (CPA) model also called the Drake model.

and $0 < M < 1$ as $\sigma_0 < \sigma_\infty$. We define the Dukhin number at low frequency as $\mathrm{Du}_0 = \sigma_S^0/\sigma_f$ and therefore we have

$$M = \frac{(F-1)f\,\mathrm{Du}_0}{1 - f + (F-1)\mathrm{Du}_0}. \tag{70}$$

This implies that at very low salinities, the chargeability can be used to compute the value of the partition of the counterions between the Stern and the diffuse layers. This is another new and important result of this work. Taking $\mathrm{Du}_0 = 1$ (surface conductivity equal to bulk pore water conductivity at low salinity, see a complete analysis in Leroy & Revil 2009), $f = 0.84$ (e.g. the value of the partition coefficient reported by Jougnot *et al.* 2009 for the Callovo–Oxfordian clay-rock), we obtain $M \approx f = 0.84$ in good agreement with the induced polarization estimates of M obtained by Ghorbani *et al.* (2009) for the same material.

3.4 Comparison with experimental results

In this subsection, we make various tests of our model to the case that is opposite to the case discussed in Section 2 that was characterized by a delta function in the particle size distribution. We consider now the case of a very broad grain size distribution. According to our model, this would yield a broad distribution of relaxation times and this explains the constant phase angle model (called the CPA or Drake model) usually used to describe the polarization spectra in such a situation (see Fig. 10 and Vinegar & Waxman 1984; Börner *et al.* 1993; Slater & Lesmes 2002b). In this case, the phase does not exhibit a well-defined relaxation time, like in Fig. 3, but a broad range of relaxation times.

The first test is related to the data reported by Slater & Lesmes (2002b, their fig. 5). In their case, the imaginary part of the conductivity shows a very weak dependence with the frequency, and according to our model, this is an indicative for a very broad
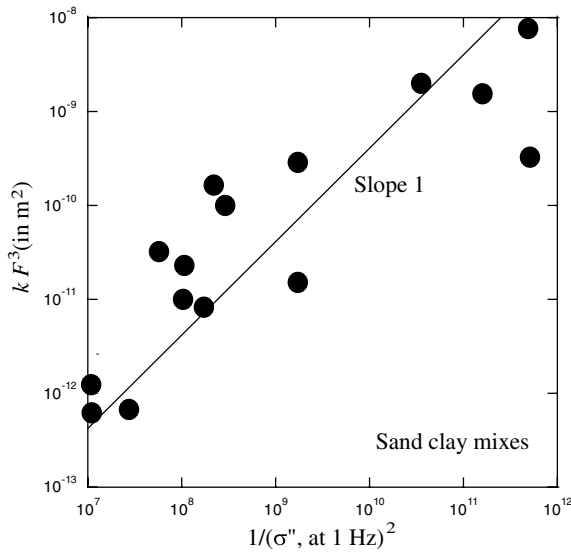
Figure 11. Comparison between the prediction of our model (the plain line with the slope -1) and the data reported by Slater & Lesmes (2002b).

distribution of grain size consistent with the use of sand clay mixtures. Using eqs (30), (37), (38), and (39), the quadrature conductivity is given by,

$$\sigma'' \sim -\frac{(F-1)\left(\sigma_S^0 - \sigma_S^\infty\right)}{F} \approx 4\Sigma^S E_h, \tag{71}$$

as $F \gg 1$. Therefore, the square of the inverse of the quadrature conductivity is proportional to,

$$1/(\sigma'')^2 \sim E_h^{-2}. \tag{72}$$

As the permeability k is proportional to the product $F^{-3} E_h^{-2}$, the product kF^3 should be proportional to $1/(\sigma'')^2$. For the sand clay mixtures reported by Slater & Lesmes (2002b), this is indeed the case as shown in Fig. 11.

A second test is performed with the dependence of the imaginary conductivity σ'' with the salinity. Slater & Lesmes (2002b, their fig. 2) showed that σ'' does not change with salinity at salinities above 0.02 mol L^{-1}. Below this salinity, σ'' decreases with salinity. According to our model, the salinity dependence of σ should be proportional to the salinity dependence of the surface conductance Σ^S. The salinity dependence of the total specific surface conductance (including the contribution from the diffuse layer) has been investigated by Revil *et al.* (1999, their fig. 5). In Fig. 12, we have reported estimates of the specific surface conductivity of the Stern layer as a function of the salinity using two datasets. As discussed by Revil *et al.* (1999), this behaviour is consistent with an electrical double layer model reported in Appendix C with reasonable values of the model parameters. This implies in turn that the quadrature conductivity can be used to diagnose the dependence of surface conductivity with the ionic strength and composition of the pore water.

We consider now the dependence of the quadrature conductivity with a mean grain size. The integral involved in the modelling of the quadrature conductivity favours the small grains and neglect the coarser grains depending of course on their overall distributions. To understand this point, let's assume that the grain size distribution is purely bimodal, with

$$f(D) = f_f \delta(D - D_f) + f_c \delta(D - D_c), \tag{73}$$
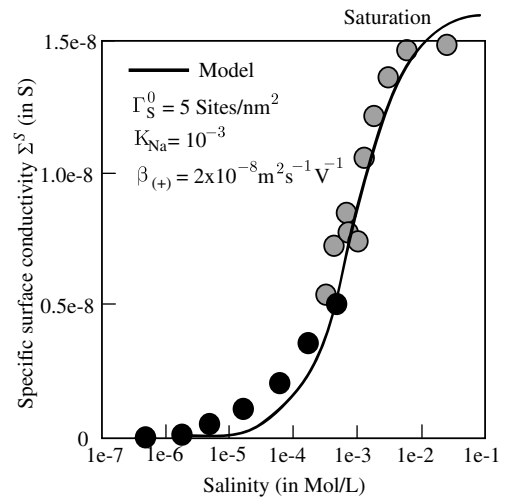
$$f_f + f_c = 1, \tag{74}$$

Figure 12. Determination of the salinity dependence of the specific surface conductivity contribution associated with the Stern layer. The black circles are determined using the data from Watillon & de Backer (1970) removing the DC contribution associated with the diffuse layer. The grey circles are determined from Slater & Lesmes (2002b, their fig. 2). The limiting value of the specific surface conductivity at high salinity is due to the close packing of the counterions on the mineral surface. The solid line corresponds to the model described in Appendix B.

where f_f is the fraction of fine grains of diameter D_f and f_c is the fraction of coarse grains of diameter D_c. With such a distribution, we have

$$E_h = \int_0^{+\infty} f(D) \mathrm{d} \ln D = \frac{f_f}{D_f} + \frac{f_c}{D_c} \approx \frac{f_f}{D_f}, \tag{75}$$

as $1/D_f \gg (f_c/f_f)(1/D_c)$. Therefore, the integral on the right-hand side of eq. (75) gives more weight to the finer grains. A complementary treatment of the problem is proposed in Appendix B for log normal and Cole–Cole grain size distributions.

Slater & Lesmes (2002b) used sand clay mixtures for which they used the effective grain diameter d_{10} at which 10 per cent of the sample is finer. If we assume that this average grain diameter is a good approximation of the grain size distribution integral involved in our modelling, we consider

$$\frac{1}{d_{10}} = \xi E_h, \tag{76}$$

where ξ is a dimensionless normalizing constant (an exact expression of this constant is given in Appendix B when the grain size distribution is given by a log normal distribution). For a binary mixture (see above) like a sand clay mixture, eqs (75) and (76) yields $\xi = 1/f_f$. Using eq. (71), we have

$$\sigma'' = \frac{4\Sigma^S}{\xi d_{10}}. \tag{77}$$

For the samples investigated by Slater & Lesmes (2002b), we have an average formation factor F of 5 ± 1. Taking $\Sigma^S = 4 \times 10^{-9}$ S (Bolève *et al.* 2007), and the correlation obtained by Slater & Lesmes (2002b, their fig. 8), we obtain σ'' (1 Hz) $= a/d_{10}$ with $a = 5 \times 10^{-10}$ S and d_{10} expressed in metres. The data of Fig. 13 yields the following value of the normalizing constant: $\xi = 4\Sigma^S/Fa = 32$. Using $f_f = 1/\xi$, this implies that 3 per cent of the grain size distribution is made of fine particles. In addition, we can use eqs (51) and (69) to compute the permeability,

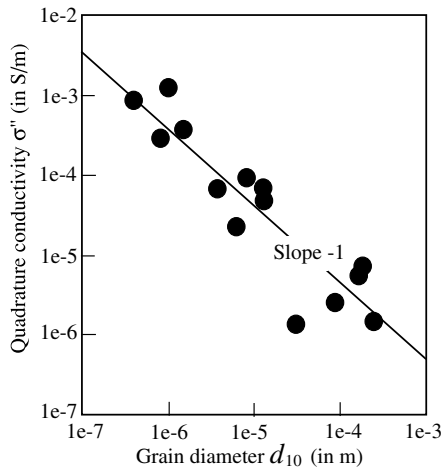$$k \approx \frac{\xi^2 d_{10}^2}{72 F^3}. \tag{78}$$

Figure 13. Relationship between the quadrature conductivity and the grain diameter d_{10} (modified from Slater & Lesmes 2002b). The line corresponds to the linear trend given by $\sigma''(1\,\text{Hz}) = a/d_{10}$ with $a = 5 \times 10^{-10}$ S and the characteristic grain diameter d_{10} expressed in meter ($R^2 = 0.83$).
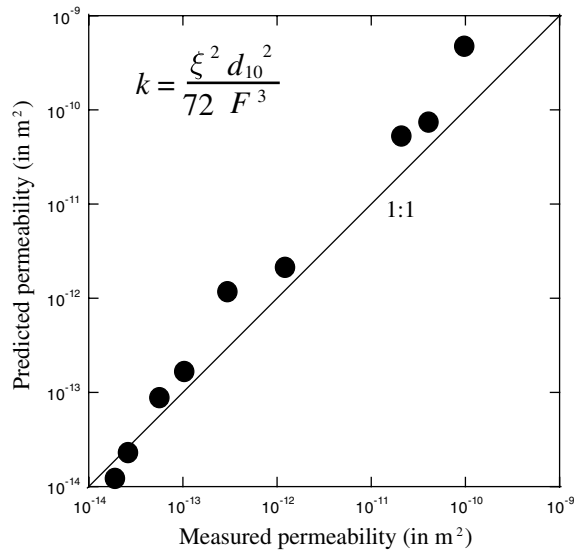

Figure 14. Comparison with the predicted permeability and the measured permeability of silts, sands, and sand till mixtures. We used the data from Slater & Lesmes (2002b, their table 1) with the formation factors and d_{10} independently measured. The predicted permeability are based on the value of ξ determined from the quadrature conductivity (see main text).

Combining eqs (77) and (78) yields also a direct relationship between the permeability and the quadrature conductivity,

$$k \approx \frac{(\Sigma^S)^2}{4.5 F^3}(\sigma'')^{-2}. \tag{79}$$

The application of this relationship to the data displayed in Fig. 11 yields $\Sigma^S = 2 \times 10^{-9}$ S, which is consistent with the data displayed also in Fig. 12. A comparison between the predicted permeability using eq. (78) and the measured permeability measured by Slater & Lesmes (2002b) is shown in Fig. 14. We found a good agreement between our model and the data.

In addition, a comparison between eq. (77) and eq. (68) explains very well the linear trends observed by Vinegar & Waxman (1984) between the quadrature conductivity σ'' and the in-phase conduc-

tivity of the solid phase σ' of shaly sandstones with kaolinite, il-lite, and smectite. According to our model, we should have $\sigma'' = (1 - f)\sigma'$. Above 1 S m^{-1}, the data by Vinegar & Waxman (1984) yield $f = 0.98$. This means that most of the counterions are located in the Stern layer at high salinities. This is consistent with the fact that the partition coefficient f increases with the salinity (see Fig. 2) and the fact that at high salinities the counterions of the diffuse layer are closely packed against the mineral surface. Indeed, the size of the diffuse layer is controlled by a length scale called the Debye length, which decreases when the salinity increases until the point where all the counterions are packed against the mineral surface (e.g. Revil & Glover 1997). Using eq. (70), this means that at high salinities (above 1 S m^{-1}), we have $M = 1$.

4 RELATION TO SURFACE AREA

The relationship between the phase or the imaginary component of the complex conductivity and the specific surface area has been widely documented in the literature (e.g. Börner & Schön 1991). If all the grains have the same size, the surface area per pore volume ratio is defined by

$$S_{\text{por}} = \frac{S}{V_p} = a\frac{1}{d_0}, \tag{80}$$

where S is the surface area between the solid phase and the water phase, V_p is the pore volume, and a is a constant that depends on the packing of the grains (for a cubic packing, a is close to 6, for instance). This model can be generalized for a general grain size distribution by

$$S_{\text{por}} = aE_h. \tag{81}$$

Now using eq. (71), for instance, we get a direct relationship between the quadrature conductivity and the specific surface area,

$$\sigma'' = \frac{4\Sigma^S S_{\text{por}}}{a}. \tag{82}$$

This formula can be compared with the formula derived empirically by Slater & Lesmes (2002) $S_{por} = b\sigma''$ with $b = 2 \times 10^9$ S^{-1}. According to our model, we have $b = a/(4\Sigma^S)$. Using $\Sigma^S = 2 \times 10^{-9}$ S implies $a = 16$, which is a reasonable value.

5 DISCUSSION

In this section, we provide a response to the following three questions: (1) what are the limitations of the present model? (2) what is the effect of a multicomponent electrolyte with respect to the case of 1:1 electrolyte (like NaCl or KCl) discussed above? and (3) how this model could be used for a permeability tomography?

(1) Regarding the limitations of the present model, it is clear that the present model is valid for granular media without the presence of fractures. The solid phase needs to be discontinuous to observe a polarization associated with the Stern layer. This includes sands, silts, clean and clayey sandstones. Our model would not work for rocks characterized by a continuous solid phase for which there is no polarization of the Stern layer. Limestone does not exhibit Stern layer polarization because, most of the time, it imposes conditions to the pore water that are close to its isoelectric point for which the total charge of the mineral surface is close to zero (Pokrovsky *et al.* 1999). In addition, our approach would not work if there are other polarization mechanisms that would hide the polarization of the Stern layer like those associated with redox effects usually characterized by non-linear induced polarization effects.

Another limitation of our model is related to the use of a linear conductivity model while a non-linear conductivity model should be used at low salinities. The linear model was used because it yields easily to analytical solutions for the in-phase and quadrature conductivities. However, a non-linear model, for example, based on differential effective medium theory, would be more accurate at low salinities.

Finally, the grain size distribution can be difficult to evaluate. For instance, the roughness of the grains can be responsible for polarization at relatively high frequencies depending on the topology of the pore water/mineral interface (see Leroy *et al.* 2008). Cemented grains can behave as coarse grains. These two effects may explain why the distribution of relaxation times seems always broader than implied from a simple estimate of the grain size distribution. Membrane polarization will need also to be investigated in detail as it may be present in the induced polarization data but not exactly at the same frequencies as the polarization associated with the electrical double layer. Indeed, the diffusion coefficient arising in the membrane polarization mechanism is the mutual diffusion coefficient of the salt, which is distinct to the diffusion coefficient of the counterions in the Stern layer. Because the relaxation time depends on the diffusion coefficient, distinct diffusion coefficients produce distinct relaxation times. Combining Stern layer and membrane polarization mechanisms may be responsible also for the broadening of the distribution of the relaxation times.

(2) The second question is also important because real pore waters are multicomponent electrolytes. Computing all the distributions of the ions in the Stern layer, the diffuse layer, and the macropores is a difficult task but we know how to handle this problem (see Leroy *et al.* 2007 for an example using the Callovo–Oxfordian clay-rock). The question is how the presence of various counterions in the Stern layer may affect the induced polarization spectra. In Appendix D, we have generalized the analysis made in Section 2 to a multicomponent electrolyte with various ions sorbed in the Stern layer. In this model, the presence of various counterions broadens the spectra. This has many implications on the way the experiments should be also made in the laboratory or interpreted. It is customary in the literature to find experiments performed with demineralized water as the saturating fluid. Usually, this creates some dissolution of the mineral surface (e.g. Leroy *et al.* 2008). This dissolution yields various types of ions to be present in the pore water solution. We advocate here that experiments should be performed with a background electrolyte dominated by a single cation. A multicomponent electrolyte may be responsible for broadening the distribution of the relaxation times.

(3) With the assumptions discussed above, we think that the theory developed in this paper could be used to develop a permeability tomography approach based on spectral induced polarization. This would imply to divide the system in a sum of individual cells and to compute for example the Cole–Cole parameters at each cell as shown for instance by Loke *et al.* (2006). Then, the present theory could be used to invert the permeability of each cell. We plan to investigate such a problem in a forthcoming work. Such an approach could be very useful to monitor for example changes in permeability associated with plugging of the pores during bioremediation or internal erosion in earth dams and should be combined also with self-potential measurements. Indeed, self-potential has appeared recently as a powerful tool to image ground water flow associated with pumping tests (Straface *et al.* 2007; Jardani *et al.* 2009; Malama *et al.* 2009a,b), at the scale of catchments (Linde *et al.* 2007), in geothermal fields (Jardani *et al.* 2008; Jardani & Revil 2009), and in embankment dams (Bolève *et al.* 2009).

6 CONCLUSIONS

The following concluding statements result from this work. (1) The Stern layer has no contribution to DC-surface conductivity because the back-diffusion of the counterions in the Stern layer prevents a DC contribution to the Stern conductivity. (2) We speculate (as there is no definitive proof) that the value of the mobility of the ions in the Stern layer is close to the value of the mobility of the ions in free water except if the counterions have a strong affinity with the mineral sites. Such an assumption seems consistent with the available experimental data but should be carefully evaluated in future works. (3) If all the grains have the same size, the permeability can be computed from the relaxation time of induced polarization and to the cube of the electrical formation factor. The mean relaxation time is related to the square of the grain diameter. (4) In the general case of a distribution of grain sizes, the permeability is still inversely proportional to the cube of the formation factor and to the expectation of the probability distribution of the inverse of the grain size. The grain size distribution is related to the distribution of the relaxation times determined from induced polarization under the condition that the polarization of the Stern layer is the dominant polarization mechanisms in the investigated frequency band. (5) For a very broad grain size distribution, the permeability can be computed from the formation factor and the quadrature conductivity, which can be nearly frequency-independent. (6) The dependence of the quadrature conductivity and relaxation time with the specific surface area are also explained by our model. (7) A theoretical justification can be given to the Cole–Cole model widely used to fit spectral induced polarization data based on the fact that the Cole–Cole probability distribution can fit the grain size distribution. (8) Membrane polarization has been neglected. However, the importance of this mechanism needs to be further assessed and the approach of Vinegar & Waxman (1984) could be used to merge the Stern layer contribution with the membrane polarization contribution into a unified model of low-frequency polarization.

REFERENCES

Archie, G.E., 1942. The electrical resistivity log as an aid in determining some reservoir characteristics, *Trans. Am. Inst. Min. Metall. Eng.,* **146,** 54–62.

Avellaneda, M. & Torquato, S., 1991. Rigorous link between fluid permeability, electrical conductivity, and relaxation times for transport in porous media, *Phys. Fluids A,* **3,** 2529–2540.

Berg, R.R., 1970. Method for determining permeability from reservoir rock properties, Trans. Gulf Coast Section, Soc. Econ. Paleont. Mineral., *Am. Ass. Petrol. Geol.,* **20,** 303–317.

Bernabé, Y. & Revil, A., 1995. Pore-scale heterogeneity, energy dissipation and the transport properties of rocks, *Geophys. Res. Lett.,* **22**(12), 1529–1552.

Binley, A., Slater, L.D., Fukes, M. & Cassiani, G., 2005. Relationship between spectral induced polarization and hydraulic properties of saturated and unsaturated sandstone, *Water Resour. Res., 41*, W12417.

Bolève, A., Crespy, A., Revil, A., Janod, F. & Mattiuzzo, J.L., 2007. Streaming potentials of granular media: influence of the Dukhin and Reynolds numbers, *J. geophys. Res., 112*, B08204, doi:10.1029/2006JB004673.

Bolève, A., Revil, A., Janod, F., Mattiuzzo, J.L. & Fry, J.-J., 2009. Preferential fluid flow pathways in embankment dams imaged by self-potential tomography, *Near Surf. Geophys., 7*(5), 447–462, doi:10.3997/1873-0604.2009012.

Börner, F. & Schön, J., 1991. A relation between the quadrature component of electrical conductivity and the specific surface area of sedimentary rocks, *Log Analyst, 32*, 612–613.

Börner, F.D., Gruhne, M. & Schön, J. H., 1993. Contamination indications derived from electrical properties in the low frequency range, *Geophys. Prospect., 41*, 83–98.

Börner, F.D., Schopper, W. & Weller, A., 1996. Evaluation of transport and storage properties in the soils and groundwater zone from induced polarization measurements, *Geophys. Prospect., 44*, 583–601, doi:10.1111/j.1365-2478.1996.tb00167.x.

Bussian, A.E., 1983. Electrical conductance in a porous medium, *Geophysics, 48*, 1258–1268.

Carrique, F., Arroyo, F.J. & Delgado, A.V., 1998. Effect of Size Polydispersity on the dielectric relaxation of colloidal suspensions: a numerical study in the frequency and time domains, *J. Colloid Interface Sci., 206*, CS985747, 569–576.

Chassagne, C., Bedeaux, D. & Koper, G.J.M., 2002. The interpretation of dielectric spectroscopy measurements on silica and hematite sols, *J. Colloid Interface Sci., 255*, 129–137, doi:10.1006/jcis.2002.8639.

Chen, Y. & Or, D., 2006. Effects of Maxwell-Wagner polarization on soil complex dielectric permittivity under variable temperature and electrical conductivity, *Water Resour. Res., 42*, W06424, doi:10.1029/2005WR004590.

Cole, K.S. & Cole, R.H., 1941. Dispersion and absorption in dielectrics. I. Alternating current characteristics, *J. Chem. Phys., 9*, 341–351.

Cosenza, P., Ghorbani, A., Florsch, N. & Revil, A., 2007. Effects of drying on the low-frequency electrical properties of Tournemire argillites, *Pure appl. Geophys., 164*(10), 2043–2066.

Cosenza, P., Ghorbani, A., Revil, A., Zamora, M., Schmutz, M., Jougnot, D. & Florsch, N., 2008. A physical model of the low-frequency electrical polarization of clay-rocks, *J. geophys. Res., 113*, B08204.

de Lima, O.A.L. & Niwas, S., 2000. Estimation of hydraulic parameters of shaly sandstone aquifers from geoelectrical measurements, *J. Hydrol., 235*, 12–26, doi:10.1016/S0022-1694(00)00256-0.

de Lima, O.A.L. & Sharma, M.M., 1992. A generalized Maxwell–Wagner theory for membrane polarization in shaly sands, *Geophysics, 57*, 431–440.

De Mey, G., 1974. Gaussian and restangular distributions of relaxation times in dispersion mechanism, *Lettera al Nuovo Cimento, 9*(16), 670–672.

Dukhin, S.S. & Shilov, V.N., 2002. Nonequilibrium electric surface phenomena and extended electrokinetic characterization of particles, in Interfacial Electrokinetics and Electrophoresis, Edited by A.V. Delgado, *Surfact. Sci. Ser., 106*, 55–85, 991 pp.

Fixman, M., 1980. Charged macromolecules in external fields. I: the sphere, *J. Chem. Phys., 72*(a), 5177–5186.

Fuoss, R.M.D. & Kirkwood, J.G., 1941. Electrical properties of solids. VIII. Dipole moments in polyvinyl chloride-diphenyl systems, *J. Am. Chem. Soc., 63*, 385–394.

Ghorbani, A., Cosenza, Ph., Revil, A., Zamora, M., Schmutz, M., Florsch, N. & Jougnot, D., 2009. Non-invasive monitoring of water content and textural changes in clay-rocks using spectral induced polarization: a laboratory investigation, *Appl. Clay Sci., 43*, 493–502.

Hördt, A., Blaschek, R., Kemna, A. & Zisser, N., 2007. Hydraulic conductivity estimation from induced polarisation data at the field scale—the Krauthausen case history, *J. appl. Geophys., 62*, 33–46.

Jardani, A. & Revil, A., 2009. Stochastic joint inversion of temperature and self-potential data, *Geophys. J. Int., 179*(1), 640–654, doi:10.1111/j.1365-246X.2009.04295.x.

Jardani, A., Revil, A., Bolève, A. & Dupont, J.P., 2008. 3D inversion of self-potential data used to constrain the pattern of ground water flow in geothermal fields, *J. geophys. Res., 113*, B09204, doi:10.1029/2007JB005302.

Jardani, A., *et al.*, 2009. Reconstruction of the water table from self potential data: a Bayesian approach, *Ground Water, 47*(2), 213–227, 2009.

Johnson, D.L., Plona, T.J. & Kojima, H., 1986. Probing porous media with 1st sound, 2nd sound, 4th sound and 3rd sound, in *Physics and Chemistry of Porous Media,* Vol. II, pp. 243–277 eds Jayanth, R., Banavar, J. and Winkler, K. W., AIP, New York.

Johnson, D.L., Koplik, J. & Dashen, R., 1987. Theory of dynamic permeability and tortuosity in fluid-saturated porous media, *J. Fluid. Mech., 176*, 379–402.

Jougnot, D., Revil, A. & Leroy, P., 2009. Diffusion of ionic tracers in the Callovo-Oxfordian clay-rock using the Donnan equilibrium model and the electrical formation factor, *Geochem. Cosmochem.Acta, 73*, 2712–2726.

Jougnot, D., Ghorbani, A., Revil, A., Leroy, P. & Cosenza, P., 2010. Spectral Induced Polarization of partially saturated clay-rocks: a mechanistic approach, *Geophys. J. Int., 180*(1), 210–224, doi:10.1111/j.1365-246X.2009.04426.x.

Kemna, A., 2000. Tomographic inversion of complex resistivity: theory and application, *PhD thesis*, Bochum University, 196pp.

Kemna, A., Münch, H.-M., Titov, K., Zimmermann, E. & Vereecken, H., 2005. Relation of SIP relaxation time of sands to salinity, grain size and hydraulic conductivity, in *Proceedings of the 11th European Meeting of Environmental and Engineering Geophysics,* Extended Abstracts: Near Surface 2005, P054.

Krumbein, W.C. & Monk, G.D., 1942. Permeability as a function of the size parameters of unconsolidated sand, *Am. Inst. Met. Engr.*, Tech. Publ.

Leroy, P. & Revil, A., 2004. A triple layer model of the surface electrochemical properties of clay minerals, *J. Colloid Interface Sci., 270*(2), 371–380.

Leroy, P. & Revil, A., 2009. A mechanistic model for the spectral induced polarization of clay material, *J. geophys. Res., 114*, B10202, doi:10.1029/2008JB006114.

Leroy, P., Revil, A., Altmann, S. & Tournassat, C., 2007. Modeling the composition of the pore water in a clay-rock geological formation (Callovo-Oxfordian, France), *Geochim. Cosmochim. Acta, 71*(5), 1087–1097, doi:10.1016/j.gca.2006.11.009.

Leroy, P., Revil, A., Kemna, A., Cosenza, P. & Ghorbani, A., 2008. Spectral induced polarization of water-saturated packs of glass beads, *J. Colloid Interface Sci., 321*, 103–117, doi:10.1016/j.jcis.2007.12.031.

Lesmes, D.P. & Morgan, F.D., 2001. Dielectric spectroscopy of sedimentary rocks, *J. geophys. Res., 106*(B7), 13 329–13 346.

Linde, N., Revil, A., Bolève, A., Dagès, C., Castermant, J., Suski, B. & Voltz, M., 2007. Estimation of the water table throughout a catchment using self-potential and piezometric data in a Bayesian framework, *J. Hydrol., 334*, 88–98.

Loke, M.H., Chambers, J.E. & Ogilvy, R.D., 2006. Inversion of 2D spectral induced polarization imaging data, *Geophys. Prospect., 54*, 287–301.

Lyklema, J., 1995. *Fundamentals of Interface and Colloid Science,* Vol. 2, Academic Press, London.

Lyklema, J., 2002. The role of surface conduction in the development of electrokinetics, in Interfacial Electrokinetics and Electrophoresis, Edited by A.V. Delgado, *Surfact. Sci. Ser., 106*, 87–97, 991pp.

Malama, B., Revil, A. & Kulhman, K.L., 2009a. A semi-analytical solution for transient streaming potentials associated with confined aquifer pumping tests, *Geophys. J. Int., 176*, 1007–1016, doi:10.1111/j.1365-246X.2008.04014.x.

Malama, B., Kuhlman, K.L. & Revil, A., 2009b. Theory of transient streaming potentials associated with axial-symmetric flow in unconfined aquifers, *Geophys. J. Int., 179*, 990–1003, doi:10.1111/j.1365-246X.2009.04336.x.

Marshall, D.J. & Madden, T.R., 1959. Induced polarization, a study of its causes, *Geophysics, 24*, 790–816.

Masch, F.D. & Denny, K.J., 1966. Grain size Distribution and its effect on the permeability of unconsolidated sands, *Water Resour. Res., 2*(4), 667–677.

Maxwell, J.C., 1892. *A Treatise on Electricity and Magnetism,* 3rd edn, Oxford University Press, London.

Nordsiek, S. & Weller, A. 2008. A new approach to fitting induced-polarization spectra, *Geophysics,* **73,** F235–F245.

O'Konski, C.T., 1960. Electric properties of macromolecules. Y. Theory of ionic polarization in polyelectrolytes, *J. Phys. Chem.,* **64,** 605–619.

Olhoeft, G.R., 1985. Low-frequency electrical properties, *Geophysics,* **50,** 2492–2503.

Pokrovsky, O. S., Schott, J. & Thomas, F., 1999. Dolomite surface speciation and reactivity in aquatic systems, *Geochim. Cosmochim. Acta,* **63,** 3133–3143.

Posadas, A.N.D., Giménez, D., Bittelli, M., Vaz, C.M.P. & Flury, M., 2001. Multifractal characterization of soil particle-size distributions, *Soil Sci. Soc. Am. J.,* **65,** 1361–1367.

Pride, S.R., 1994. Governing equations for the coupled electromagnetics and acoustics of porous media, *Phys. Rev. B,* **50,** 15 678–15 696.

Revil, A., 1999. Ionic diffusivity, electrical conductivity, membrane and thermoelectric potentials in colloids and granular porous media: a unified model, *J. Colloid Interface Sci.,* **212,** 503–522.

Revil, A., 2007. Comment on 'Permeability prediction from MICP and NMR data using an electrokinetic approach', *Geophysics,* **72**(4), doi:10.1190/1.2743006.

Revil, A. & Cathles, L.M., 1999. Permeability of shaly sands, *Water Resour. Res.,* **35**(3), 651–662.

Revil, A. & Glover, P.W.J., 1997. Theory of ionic surface electrical conduction in porous media, *Phys. Rev. B,* **55**(3), 1757–1773.

Revil, A. & Glover, P.W.J., 1998. Nature of surface electrical conductivity in natural sands, sandstones, and clays, *Geophys. Res. Lett.,* **25**(5), 691–694.

Revil, A. & Leroy, P., 2001. Hydroelectric coupling in a clayey material, *Geophys. Res. Lett.,* **28**(8), 1643–1646.

Revil, A. & Leroy, P., 2004. Governing equations for ionic transport in porous shales, *J. geophys. Res.,* **109,** B03208, doi: 10.1029/2003JB002755.

Revil, A. & Linde, N., 2006. Chemico-electromechanical coupling in microporous media, *J. Colloid Interface Sci.,* **302,** 682–694.

Revil, A., Cathles, L.M., Losh, S. & Nunn, J.A., 1998. Electrical conductivity in shaly sands with geophysical applications, *J. geophys. Res.,* **103**(B10), 23 925–23 936.

Revil, A., Pezard, P.A. & Glover, P.W.J., 1999. Streaming potential in porous media. 1. Theory of the zeta-potential, *J. geophys. Res.,* **104**(B9), 20 021–20 031.

Revil, A., Hermitte, D., Spangenberg, E. & Cochémé, J.J., 2002. Electrical properties of zeolitized volcaniclastic materials, *J. geophys. Res.,* **107**(B8), 2168, doi:10.1029/2001JB000599.

Revil, A., Leroy, P., Ghorbani, A., Florsch, N. & Niemeijer, A.R, 2006. Compaction of quartz sands by pressure solution using a Cole–Cole distribution of relaxation times, *J. geophys. Res.,* **111,** B09205, doi:10.1029/2005JB004151.

Scott, J. & Barker, R., 2003. Determining pore-throat size in Permo-Triassic sandstones from low-frequency electrical spectroscopy, *Geophys. Res. Lett.,* **30**(9), 1450.

Scott, J. & Barker, R., 2005. Characterization of sandstone by electrical spectroscopy for stratigraphical and hydrogeological investigation, *Q. J. Eng. Geol. Hydrogeol.,* **38,** 143–154.

Sen, P.N., Scala, C. & Cohen, M.H., 1981. A self-similar model for sedimentary rocks with application to the dielectric constant of fused glass beads, *Geophysics,* **46**(5), 781–795.

Schurr, J.M., 1964. On the theory of the dielectric dispersion of spherical colloidal particals in electrolyte solution, *J. Phys. Chem.,* **68,** 2407–2413.

Schwarz, G., 1962, A theory of the low-frequency dielectric dispersion of colloidal particles in electrolyte solution, *J. Phys. Chem.,* **66,** 2636–2642.

Slater, L. & Lesmes, D., 2002a, IP interpretation in environmental investigations, *Geophysics,* **67**(1), 77–88.

Slater, L. & Lesmes, D., 2002b. Electrical-hydraulic relationships observed for unconsolidated sediments, *Water Resour. Res.,* **38**(10), 1213, doi:10.1029/2001WR00107.

Straface, S., Falico, C., Troisi, S., Rizzo, E. & Revil, A., 2007. An inverse procedure to estimate transmissivities from heads and SP signals, *Ground Water,* **45**(4), 420–428.

Sturrock, J.T., 1999. Predictions of hydraulic conductivity using spectral induced polarizations, *MS dissertation*. Boston College.

Swan, H.P., 2000. Dielectric spectroscopy of biological materials and field interactions: the connection with Gerhard Schwarz, *Biophys. Chem.,* **85,** 273–278.

Tarasov, A. & Titov, K. 2007. Relaxation time distribution from time domain induced polarization measurements, *Geophys. J. Int.,* **170,** 31–43.

Titov, K., Komarov, V., Tarasov, V. & Levitski, A., 2002. Theoretical and experimental study of time domain induced polarization in water-saturated sands, *J. appl. Geophys.,* **50,** 417– 433.

Tong, M., Li, L., Wang, W. & Jiang, Y., 2006a. Determining capillary-pressure curve, pore size distribution and permeability from induced polarization of shaley sand, *Geophysics,* **71,** N33–N40.

Tong, M., Li, L., Wang, W. & Jiang, Y., 2006b. A time-domain induced-polarization method for estimating permeability in a shaly sand reservoir, *Geophys. Prospect.,* **54,** 623–631.

Tournassat, C., Chapron, Y., Leroy, P., Bizi, M. & Boulahya, F., 2009. Comparison of molecular dynamics simulations with triple layer and modified Gouy-Chapman models in 0.1 M NaCl-montmorillonite system, *J. Colloid Interface Sci.,* **339**(2), 533–541.

Vinegar, H.J. & Waxman, M.H., 1984. Induced polarization of shaly sands, *Geophysics,* **49,** 1267–1287.

Wagner, K.W., 1914. Erklärung der dielektrischen Nachwirkungsvorgänge auf Grund Maxwellscher Vorstellungen, *Archiv. Electrotechnik,* **2,** 371–387.

Watilion, A. & De Backer, R., 1970. Potentiel d'écoulement, courant d'écoulement et conductance de surface à l'interface eau-verre, *J. Electroanal. Chem., Interfacial Electrochem.,* **25,** 181–196.

Waxman, M.H. & Smits, L.J.M., 1968. Electrical conductivities in oil bearing shaly sands, *Soc. Pet. Eng. J.,* **8,** 107–122.

Yeung, Y.Y. & Shin, F.G., 1991. Pulse response function of dielectric susceptibility, *J. Mater. Sci.,* **26,** 1781–1787.

Yukselen, Y. & Kaya, A., 2008. Suitability of the methylene blue test for surface area, cation exchange capacity and swell potential determination of clayey soils, *Eng. Geol.,* **102,** 38–45.

Zisser, N., Kemna, A. & Nover, G., 2009. Relationship between low-frequency electrical properties and hydraulic permeability of low-permeable sandstones, *Geophysics,* in press.

Zukoski, C.F. & Saville, D.A., 1986a. The interpretation of electrokinetic measurements using a dynamic model of the stern layer. I. the dynamic model, *J. Colloid Interface Sci.,* **114**(1), 32–44.

Zukoski, C.F. & Saville, D.A., 1986b. The interpretation of electrokinetic measurements using a dynamic model of the stern layer. II. Comparisons between theory and experiments, *J. Colloid Interface Sci.,* **114**(1), 45–53.

APPENDIX A: DERIVATION OF THE WAXMAN AND SMITS EQUATION

We consider a two-phase porous material for which the DC electrical conductivity σ_0 is given by a simple phase average of the conductivity of the fluid saturating the pores σ_f and the conductivity of the solid phase σ_S^0

$$\sigma_0 = \phi \sigma_f + (1 - \phi)\sigma_S^0. \tag{A1}$$

However this equation is not consistent with Archie's law

$$\lim_{\sigma_S^0 \to 0} \sigma_0 = \frac{1}{F}\sigma_f = \phi^m \sigma_f. \tag{A2}$$

In addition, we can interpret the inverse of the formation factor as an effective porosity as discussed by Revil & Cathles (1999). This effective porosity is often called the mobile porosity in reactive transport modelling and the difference $(\phi - 1/F)$ corresponds to the so-called immobile porosity. The porosity of the simple (and somehow naive) phase average in eq. (A1) should be therefore replaced by the inverse of the formation factor,

$$\sigma_0 = \frac{1}{F}\sigma_f + \left(1 - \frac{1}{F}\right)\sigma_S^0, \tag{A3}$$

and now eq. (A3) is consistent with eq. (A2). Algebraic manipulations of eq. (A3) yields

$$\sigma_0 = \frac{\sigma_f}{F} \left[1 + (F - 1)\mathrm{Du}_0 \right], \tag{A4}$$

$$\mathrm{Du}_0 = \frac{\sigma_S^0}{\sigma_f}, \tag{A5}$$

where Du_0 is a dimensionless parameter called the Dukhin number in honour of the great Russian electrochemist S. S. Dukhin who pioneered the study of surface conductivity in colloidal science (Lyklema, 1995). This dimensionless number is defined as the ratio of the solid to fluid conductivities. In the case of a granular material with insulating grains coated by the electrical double layer, the Dukhin number can be related to the excess of charge per unit volume by (Bolève *et al.* 2007)

$$\mathrm{Du}_0 = \frac{4\Sigma^d}{d_0 \sigma_f} = \frac{2}{3} \left(\frac{\phi}{1 - \phi} \right) \frac{\beta_{(+)} \bar{Q}_V}{\sigma_f}, \tag{A6}$$

where $\beta_{(+)}$ is the mobility for the counterions in the diffuse layer (see Section 2). At high porosity, we can now demonstrate that eqs (A4) to (A5) yield a Waxman and Smits-type equation (Waxman & Smits, 1968). At high porosity and for a granular material, the formation factor is given from the effective medium theory (Sen *et al.* 1981) by $F = \phi^{-3/2}$, which is an Archie-type relationship with a cementation exponent of 1.5. A Taylor expansion of the previous Archie's law at high porosities yields

$$F = 1 + \frac{3}{2} \left(\frac{1 - \phi}{\phi} \right) + \cdots, . \tag{A7}$$

Inserting eqs (A7) and (A6) into (A4) results in the following Waxman and Smits-type equation,

$$\sigma_0 = \frac{1}{F} (\sigma_f + \beta_S Q_V), \tag{A8}$$

where $\beta_S = \beta_{(+)} (1 - f)$, f being the fraction of the counterions located in the Stern layer. Revil & Linde (2006) obtained also eq. (A8) using a volume-averaging method. This means that eq. (A8) seems to be valid in a wide range of porosity. However, this equation is only valid at relatively high salinities as discussed by Bernabé & Revil (1995) who performed numerical simulations of the DC electrical conductivity with a pore network model.

APPENDIX B: PERMEABILITY OF A BROAD GRAIN SIZE DISTRIBUTION

We consider first the log normal distribution for the probability density $F(s)$

$$\int_{-\infty}^{+\infty} F(s) \mathrm{d}s = 1, \tag{B1}$$

$$F(s)\mathrm{d}s = \frac{1}{\sqrt{2\pi}\hat{\sigma}} \exp \left[- \left(\frac{s}{\sqrt{2}\hat{\sigma}} \right)^2 \right] \mathrm{d}s, \tag{B2}$$

where $s = 2 \ln (D/d_{50})$ (d_{50} represents the median of the grain size distribution).

In this Appendix, we are interested to estimate the integral

$$E_h = \int_0^{+\infty} f(D) \mathrm{d} \ln D, \tag{B3}$$

with the probability density function $f(D)$ given as a log normal distribution. Replacing s by $s = 2 \ln (D/d_{50})$ in eq. (B2), we have

$$f(D) = \frac{1}{D\sqrt{2\pi}\sigma} \exp \left[-\frac{(\ln D - \mu)^2}{2\sigma^2} \right], \tag{B4}$$

$$\int_0^{+\infty} f(D)\mathrm{d}D = 1, \tag{B5}$$

with $\sigma = \hat{\sigma}/2$ and $\mu = \ln d_{50}$ are the standard deviation and the mean of the grain diameter natural logarithm, respectively, and d_{50} represents the median of the grain size distribution. The median d_{50} is used as a measure of the average particle diameter size for the granular material. The standard deviation represents a measure of the dispersion about the mean grain diameter for a given distribution. We first demonstrate that E_h is nothing else that the expected value of the distribution $h(\eta)$ with η being the inverse of the grain diameter $\eta = 1/D$ (see Section 3.1). Indeed, E_h is defined by

$$E_h \equiv \int_0^{+\infty} \eta h(\eta) \, |\mathrm{d}\eta| \, . \tag{B6}$$

Using $h(\eta)|\mathrm{d}\eta| = f(D)\mathrm{d}D$ and $\eta = 1/D$ in eq. (B6) yields eq. (B3). Therefore, eqs (B3) and (B6) are formally equal to each other.

Integrating eq. (B3) with eq. (B4) yields

$$E_h = \exp \left(\frac{1}{2}\sigma^2 - \mu \right), \tag{B7}$$

$$E_h = \frac{1}{d_{50}} \exp \left(\frac{1}{2}\sigma^2 \right). \tag{B8}$$

Inserting eq. (B8) into the expression of the permeability, eq. (55), we obtain

$$k = \frac{1}{72} \phi^{3m} d_{50}^2 \exp(-\sigma^2). \tag{B9}$$

When $\sigma = 0$, we recover the formula obtained for a delta distribution in the grain size distribution (eq. 14, for instance). Eq. (B6) can be directly compared to the empirical formula derived by Berg (1970)

$$k = \frac{1}{12} \phi^{5.1} d_{50}^2 \exp (-\Delta_{\ln D}), \tag{B10}$$

where $\Delta_{\ln D}$ is a permeability reduction factor corresponding to the measure of the spread of the grain size distribution on a log scale (see also Kemna, 2000). To our knowledge, this idea to scale the permeability with an exponential function of the standard deviation of the grain size distribution was first proposed by Krumbein and Monk (1942). Eq. (B9) is also consistent with the analysis made by Mash and Denny (1966) regarding the influence of the median and the standard deviation of the grain size distribution upon the permeability. Note also that the sorting coefficient, defined as $S_0 = (D_{25}/D_{75})^{1/2}$ can be directly related to σ by $S_0 = \exp(0.674\sigma)$. A very poorly sorted sand is defined by $S_0 = 4.2$, which means that $\sigma = 2.13$, and therefore the permeability reduction factor $\vartheta = \exp(-\sigma^2)$ in eq. (B9) is equal to $\exp(-4.5)$, a very low value. So our model can be used to analyse quantitatively how sorting influences permeability.

Assuming a log normal grain size distribution, the parameter ξ defined by eq. (76), can now be defined by

$$\xi = \frac{d_{50}}{d_{10}} \exp \left(-\frac{1}{2}\sigma^2 \right), \tag{B11}$$

and therefore ξ is proportional to a coefficient of uniformity, which is rigorously defined in soil sciences as $U = d_{60}/d_{10}$ where coefficient d_{60} is the value of the particle diameter such that 60 per cent of the distribution is finer than this diameter and d_{10} is the value of the particle diameter such that 10 per cent of the distribution is finer than this diameter (Mash & Denny 1966).

We consider now the case of a Cole–Cole distribution

$$F(s)ds = \frac{1}{2\pi} \frac{\sin[\pi(1-\alpha)]}{\cosh[\alpha s] - \cos[\pi(1-\alpha)]} ds. \tag{B12}$$

It follows that

$$f(D) = \frac{1}{\pi D} \frac{\sin[\pi(1-\alpha)]}{\cosh[2\alpha \ln(D/d_{50})] - \cos[\pi(1-\alpha)]}, \tag{B13}$$

$$\int_0^{+\infty} f(D)dD = 1. \tag{B14}$$

In the case of a Cole–Cole distribution, getting an analytical solution for E_h is a much more difficult task than for the log normal distribution. Using the change of variables $x = D/d_{50}$, E_h is given by

$$E_h = \frac{1}{d_{50}} \frac{\sin[\pi(1-\alpha)]}{\pi} \int_0^\infty \frac{dx}{x^2 [\cos(2\alpha \ln x) - \cos[\pi(1-\alpha)]]}. \tag{B15}$$
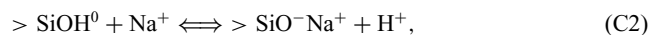
With the additional assumption that $\alpha > 1/2$, we can find an approximate solution of the integral involved in eq. (B15) using a polynomial expansion of the integrand. This yields

$$E_h \approx \frac{1}{\pi d_{50}} \left\{ \frac{2\sin[\pi(1-\alpha)]}{(2\alpha - 1)} + a_3 \alpha^3 + a_2 \alpha^2 + a_1 \alpha + a_0 \right\}, \tag{B16}$$

with $a_0 = -8.9971$, $a_1 = 26.8834$, $a_2 = -20.8123$ and $a_3 = 6.0676$. We can first check that if $\alpha = 1$, the Cole–Cole model should be equal to a Delta distribution and indeed taking $\alpha = 1$ in (B16) yields $E_h = 1/d_{50}$ (the expectation E_h is equal to the inverse of the mean of the grain diameter distribution).

APPENDIX C: THE CONDUCTANCE OF THE STERN LAYER

We consider that the sorption of sodium in the Stern layer on a silica grain can be represented by the following reaction:

$$> SiOH^0 \Longleftrightarrow > SiO^- + H^+, \tag{C1}$$

$$> SiOH^0 + Na^+ \Longleftrightarrow > SiO^-Na^+ + H^+, \tag{C2}$$

where the equilibrium constants are defined by

$$K_{(-)} = \frac{\Gamma^0_{SiO^-} [H^+]^0}{\Gamma^0_{SiOH}}, \tag{C3}$$

$$K_{Na} = \frac{\Gamma^0_{SiONa} [H^+]^0}{\Gamma^0_{SiOH} [Na^+]^0}, \tag{C4}$$

where Γ^0_i is the surface concentration of species i in the Stern layer and $K_{(-)} = 10^{-7.4}$ at 25 °C. Fitting an adsorption isotherm and solving the equation of the electrical double layer, Revil *et al.* (1999) found that $K_{Na} = 10^{-3.25}$ at 25 °C and pH = 6. At pH = 6, we can simplify the formula derived by Revil *et al.* (1999) to model the Stern layer conductivity as a function of the salinity C_f. We obtain

$$\Sigma^S = e\beta_{(+)} \Gamma^0_S \frac{K_{Na} C_f}{10^{-pH} + K_{Na} C_f}, \tag{C5}$$

where the total site density Γ^0_S is typically equal to five sites nm^{-2}. This yields $e \Gamma^0_S = 0.8$ C m^2. Using these values and reasonable values for the mobility of the counterions, we can compute the dependence of the specific surface conductance of the Stern layer as a function of the salinity.

APPENDIX D: GENERALIZATION TO A MULTICOMPONENT ELECTROLYTE

The equations of the main text have been developed for a binary symmetric 1:1 electrolyte. These equations can be however generalized to a multicomponent electrolyte. Eq. (19), for a 1:1 electrolyte, can be expressed more explicitly as

$$\sigma_S = \frac{4}{d_0} \left(\Sigma^d + e\beta_{(+)} \Gamma^0_{(+)} \right) - \frac{4}{d_0} \frac{e\beta_{(+)} \Gamma^0_{(+)}}{1 + i\omega \left(\frac{ed_0^2}{8k_b T \beta_{(+)}} \right)}, \tag{D1}$$

where $\Gamma^0_{(+)}$ represents the fraction of counterions sorbed in the Stern layer per unit surface area. Eq. (D1) can be easily generalized to a multicomponent electrolyte

$$\sigma_S = \frac{4}{d_0} \left(\Sigma^d + \sum_{i=1}^Q e\beta_i \Gamma^0_i \right) - \frac{4}{d_0} \sum_{i=1}^Q \frac{e\beta_i \Gamma^0_i}{1 + i\omega \tau^0_i}. \tag{D2}$$

$$\tau^0_i = \frac{ed_0^2}{8k_b T \beta_i}, \tag{D3}$$

where Γ^0_i represents the fraction of counterions of species i sorbed in the Stern layer per unit surface area. These parameters can be obtained from a multicomponent triple layer model (e.g. Leroy *et al.* 2007).

Eq. (D2) implies that different relaxation processes may overlap in the frequency domain because of the different mobilities of the counterions located in the Stern layer resulting in different main relaxation time constants. The result will be a broader dispersion of the electrochemical polarization in the frequency domain. Therefore, performing experiments at ionic strengths with a multicomponent electrolyte does not produce the same spectrum as using a 1:1 dissociated salt at the same electrical conductivity. Interpreting therefore induced polarization data with a simple model valid for a 1:1 electrolyte may be grossly wrong as well as the estimate of the resulting grain size distribution from the distribution of the relaxation times.